



Statistical Evaluation of Seismic Velocity Models of Permafrost

Xiaohang Ji, S.M.ASCE1; Ming Xiao, F.ASCE2; Eileen R. Martin3; and Tieyuan Zhu4

Abstract: The warming climate in high-latitude permafrost regions is leading to permafrost degradation. Estimating seismic wave velocities in permafrost could help predict the geomechanical properties of permafrost and provide information to plan and design resilient civil infrastructure in cold regions. This paper evaluates the performance of seven models when predicting the seismic wave velocities of permafrost statistically; these models are the time-average, Zimmerman and King, Minshull et al., weighted equation, three-phase, Biot-Gassmann theory modified by Lee (BGTL), and Dou et al. models. The data used in the evaluation are from published laboratory and in situ data, which includes 369 data points for joint P and S wave velocities from nine publications and 943 unfrozen water content data points from 12 publications. The unfrozen water content that is used in these models is determined from a modified Dall'Amico's model that is proposed, which is evaluated against six existing unfrozen water content models based on soil temperature. This paper finds that saturated nonsaline permafrost generally shares similar linear trends between the P and S wave velocities, regardless of soil type, porosity, grain size, and temperature. Fitting all existing data, an empirical linear relationship is derived between the P and S wave velocities. Among the seven models evaluated, the Minshull et al. and BGTL models are the most accurate when predicting the seismic velocities of permafrost. **DOI:** 10.1061/JCRGELCRENG-760. © 2024 American Society of Civil Engineers.

Practical Applications: Unfrozen water content and seismic wave velocity models are valuable tools for quantitatively predicting permafrost dynamics and degradation, with practical applications in various engineering areas with permafrost environments. As permafrost thaws due to rising temperatures, these models could be used to guide the quantitative interpretation of geophysical changes in subsurface conditions, assess the potential for ground instability, and predict future permafrost degradation. Unfrozen water content models are used to predict the percentage of unfrozen water within permafrost, which links the changes with permafrost temperature. Unfrozen water content models of permafrost are essential when assessing permafrost thaw, thermal performance, heat transfer processes in permafrost, and the effect of civil infrastructure on permafrost (Chen et al.,). The seismic wave velocity models could help engineers assess the subsurface conditions in permafrost areas; this assessment is crucial for environmental and seismic monitoring, land use planning, infrastructure design and construction, and natural resources exploration.

Author keywords: Permafrost; Seismic velocity; Statistical evaluation; Unfrozen water content.

Introduction

Increasing air temperatures are driving permafrost warming across high-latitude permafrost regions. As permafrost warms, its geomechanical properties degrade, which leads to permafrost degradation that disrupts natural ecosystems and infrastructure systems and results in enduring societal consequences. Studying the geomechanical properties of permafrost could improve the quantitative prediction of permafrost warming. The geomechanical properties

¹Graduate Student, Dept. of Civil and Environmental Engineering, Pennsylvania State Univ., University Park, PA 16802 (corresponding author). ORCID: https://orcid.org/0000-0002-1607-662X. Email: xhji@psu.edu

Note. This manuscript was submitted on June 22, 2023; approved on January 10, 2024; published online on June 11, 2024. Discussion period open until November 11, 2024; separate discussions must be submitted for individual papers. This paper is part of the *Journal of Cold Regions Engineering*, © ASCE, ISSN 0887-381X.

of permafrost include strength characteristics, such as compressive, tensile, yield, and shear strengths, and elastic moduli, such as bulk, shear, Young's, and Poisson's ratio. The acquisition of these geomechanical properties requires accessing and sampling permafrost using borehole drilling and laboratory testing, which could be difficult, expensive, and time-consuming (Ferrero et al. 2014). Observations that are based on sampling are limited due to a limited number of sites, and the heterogeneity of permafrost leads to potentially significant variations in conditions within a short distance (e.g., near the edge of an ice wedge). In addition, many studies were based on remolded, artificially frozen soil samples, which might not represent field conditions (Yang et al. 2015). For instance, the shear strength of frozen soil is influenced by the sample preparation method, which includes freezing conditions, strain rate, and sample orientation and size (Radd and Wolfe 1979). Therefore, to understand the in situ geomechanical properties, in situ measurement techniques are preferred.

Seismic wave velocities that are estimated using in situ measurements could be used to indicate the in situ strength and moduli of soils. Previous studies found that seismic wave velocities correlated with the compressive strength of permafrost (Schön 2011; Dou et al. 2016), because seismic wave propagation is affected by external stresses in permafrost (i.e., compressive, tensile, and shear). In addition, previous laboratory tests demonstrated that the geomechanical strengths and seismic wave velocities are

²Professor, Dept. of Civil and Environmental Engineering, Pennsylvania State Univ., University Park, PA 16802. Email: mzx102@psu.edu

³Assistant Professor, Dept. of Geophysics and Applied Math and Statistics, Colorado School of Mines, Golden, CO 80401. ORCID: https://orcid.org/0000-0002-3420-4971. Email: eileenrmartin@mines.edu

⁴Associate Professor, Dept. of Geosciences, Pennsylvania State Univ., University Park, PA 16802. Email: tyzhu@psu.edu

affected by temperature variations (Ferrero et al. 2014). For instance, the elastic modulus and compressive strength of permafrost increase with decreasing temperature (Yang et al. 2015; Haynes and Karalius 1977; Zhu and Carbee 1984; Liew et al. 2022). The elastic modulus can be calculated based on seismic wave velocities

$$K = \rho \left(V_p^2 - \frac{4}{3} V_s^2 \right) \tag{1}$$

$$G = \rho V_s^2 \tag{2}$$

$$E = \frac{\rho V_s^2 (3V_p^2 - 4V_s^2)}{V_p^2 - V_s^2} \tag{3}$$

$$\nu = \frac{V_p^2 - 2V_s^2}{2(V_p^2 - V_s^2)} \tag{4}$$

where V_p = compressional wave velocity (m/s); V_s = shear wave velocity (m/s); K = bulk modulus (Pa): G = shear modulus (Pa); ρ = bulk density of a soil specimen(g/m³); E = Young's modulus (Pa); and v = Poisson's ratio.

Seismic methods allow maps of in situ permafrost geomechanical properties to be reconstructed in larger regions and identify the heterogeneity of permafrost. These methods could be used to study the temporal changes in permafrost, the distribution of the active and permafrost layers, talik formation, thermokarst, and ice wedges. Previous laboratory tests have shown an apparent increase in seismic wave velocities in permafrost as the temperature decreased below 0°C (Nakano et al. 1972; Kurfurst 1976; King et al. 1988). The increase correlates with the increase in ice content (Timur 1968; Nakano and Froula 1973; Zimmerman and King 1986), which is equivalent to the decrease in unfrozen water content (King et al. 1988; Leclaire et al. 1994). Therefore, seismic wave velocities could be quantified based on ice content and water saturation using seismic wave velocity models. However, establishing a precise quantitative relationship between the seismic velocities and ice content is challenging due to the substantial influence of the ice microstructure (Dou et al. 2017).

Thimus et al. (1991) and Lyu et al. (2020) evaluated seismic wave velocity models to determine the unfrozen water content. Thimus et al. (1991) compared Boom clay between the three-phase Wood's and time-average equations and the Zimmerman and King (1986) model. Lyu et al. (2020) evaluated eight seismic wave velocity models that related seismic wave velocities to unfrozen water content and summarized the limitations and applications of each model. Carcione and Seriani (1998) evaluated six seismic wave velocity models, which included the Voigt (Voigt 1928) and Reuss (Reuss 1929) models and the three-phase Biot theory that was proposed by Leclaire et al. (1994). Building on the findings of these previous evaluation studies, models that are suitable for permafrost will be assessed in this paper. The Voigt and the Reuss models are excluded from the scope of this paper, because they could be applied to all viscoelastic composite materials, which encompasses a broader range than permafrost.

Of note, all seismic velocity models that are discussed in this paper assume saturated permafrost and are based on the volumetric proportions of the three permafrost constituents: (1) soil grains; (2) unfrozen water; and (3) ice. Therefore, these seismic velocity models employ ice and unfrozen water contents as inputs. Unfrozen water in frozen soil is the amount of liquid water that remains at a negative temperature due to capillarity and the surface potential energy of the soil (Hu et al., 2020). The volumetric unfrozen water content could be used to reflect the volumetric proportions

of the unfrozen water content and ice and to calculate the volumetric proportion of the soil grains. In addition, the unfrozen water content significantly influences the thermo-hydro-mechanical (THM) behavior of frozen soils (Lyu et al. 2020) and plays an important role when determining the responses of seismic wave velocities and geomechanical property changes to thermal perturbations (Dou et al. 2016, 2017); therefore, exerting an impact on permafrost's seismic wave velocities and geomechanical properties. As the unfrozen water content changes, the volume proportions of unfrozen water and ice alter and strongly influence the mechanics of frozen soil and, therefore, seismic wave velocities. The unfrozen water content decreases with the decrease in temperature (Watanabe and Osada 2017). The connection between seismic wave velocities and temperature variation could be achieved using the unfrozen water content models. By integrating the seismic wave velocity with the unfrozen water content models, the prediction results could establish the relationship between the seismic wave velocities and temperature.

This paper aims to evaluate seven seismic velocity models that use the unfrozen water content as the input parameter: (1) timeaverage (Wyllie et al. 1958); (2) Zimmerman and King (1986); (3) Minshull et al. (1994); (4) weighted equation (Lee et al. 1996); (5) three-phase (Leclaire et al. 1994); (6) Biot-Gassmann theory (BGTL) modified by Lee (Lee 2002); and (7) two endmember (Dou et al. 2017). These models calculate the P or S wave velocities or the composite elastic moduli of permafrost based on different theoretical assumptions. Based on the evaluation, the performance and applications of these seismic wave velocity models are summarized. The empirical relationship between the P and S wave velocities of saturated permafrost that is based on 369 data points is derived, which could provide valuable information for the study of permafrost and engineering applications. To provide unfrozen water content estimations, a modified and simpler unfrozen water content model is proposed that is based on Dall'Amico's model, which is evaluated with six existing unfrozen water content models that use 943 data points.

Reviews of Existing Unfrozen Water Content Models and Seismic Wave Velocity Models Applied in Permafrost

Reviews of Existing Unfrozen Water Content Models in Permafrost

Unfrozen water content is determined using soil temperature, the specific surface area of soil particles, the soil-water characteristic curve, or different types of water (e.g., free, capillary, and bound) (Hu et al. 2020; Li et al. 2023a, in press). The models that use soil temperature are relatively easy to implement when predicting seismic wave velocity. Therefore, in this section, six commonly used unfrozen water content models that use soil temperature are reviewed, which include Michalowski (1993), McKenzie et al. (2007), Kozlowski (2007), Anderson and Tice (1972), Zhang et al. (2017), and Dall'Amico et al. (2011) (Appendix I). The soil parameters used in these models that are listed in Appendix I include volumetric unfrozen water content $[\theta_u]$ $((V_u)/(V))$] (where the volume of unfrozen water is V_u and the total volume of frozen soil including the pore space is V), water freezing temperature (T_t) , initial volumetric water content (θ_0) at T_f , residual volumetric water content (θ_{res}), and soil—water potential energy as a function of temperature $[\Psi(T)]$ [Eq. (9)].

The models by Anderson and Tice (1972), Michalowski (1993), and Kozlowski (2007) are initially expressed by gravimetric

unfrozen water content. These values are converted into volumetric unfrozen water content, as shown in Eq. (8). For nonsaline soil, $T_f = 0^{\circ}\text{C}$ is used. The residual volumetric unfrozen water content (θ_{res}) is the unfreezable water content at a low temperature (T_{res}). The temperature of T_{res} is usually below -10°C , at which the unfrozen water content is constant or has small changes (Kozlowski 2007).

The unfrozen water content models listed in Appendix I include empirical and semitheoretical models. The empirical models, such as those that use soil temperature, are easy to implement in numerical modeling with simple formulas. Their limitations are that the fitting parameters lack physical meaning (Hu et al. 2020; Li et al. 2023a, in press), and the parameters vary between soil samples. Lu et al. (2019) discussed the influence of fitting parameters and the boundary conditions of the Michalowski (1993), McKenzie et al. (2007), Kozlowski (2007), Anderson and Tice (1972), and Zhang et al. (2017) models. Semitheoretical unfrozen water content models provide relatively accurate results; however, they present challenges due to their complexity and difficulty in practical applications and numerical modeling (Hu et al. 2020). For instance, the models that use soil-water characteristic curves are semitheoretical models that were established based on van Genuchten equation (van Genuchten 1980) and the Clapeyron equation (Dall'Amico et al. 2011; Ren et al. 2017; Li et al. 2023a, in press; Li et al. 2023b). Although these models provide enhanced accuracy for unsaturated soils by considering suction, they require more input properties and entail a longer computation time compared with empirical models. Therefore, simplified models are frequently employed in applications (Li et al. 2023a, in press).

The most common model by Anderson and Tice (1972) is an empirical power function that fits the relationship between unfrozen water content and negative temperature. However, the model prediction approaches infinity when the temperature is close to 0°C, which makes it unreasonable for conditions that are frequently encountered in polar regions. For the McKenzie et al. (2007) and Kozlowski (2007) models with $\varepsilon > 1$ (Appendix I), the derivative of the unfrozen water content curve at the freezing point is zero; this means that the unfrozen water content remains constant near

the freezing point, a behavior that is inconsistent with the actual rapid decrease in unfrozen water content during freezing (Lu et al. 2019). The unfrozen water content curve slightly varies during a freezing—thawing process (Zhang et al. 2020; Li and Li 2023), which is referred to as the freezing—thawing hysteresis. The freezing—thawing hysteresis is not considered in the unfrozen water content models that are evaluated in this paper.

Review of Existing Seismic Wave Velocity Models in Permafrost

The seismic wave velocity models that are discussed in this paper assume that the composite density is the volume-weighted average of the densities of the constituents given by

$$\rho = \phi_w \rho_w + \phi_i \rho_i + \phi_s \rho_s \tag{5}$$

where ϕ_w , ϕ_i , and ϕ_s = volume proportions of unfrozen water, ice, and soil solids, respectively; and $\phi_w + \phi_i + \phi_s = 1$. Then, ϕ_w , ϕ_i , and ϕ_s can be derived based on unfrozen water content [i.e., $\phi_w = \theta_u$, $\phi_i = \theta_0 - \theta_u$, and $\phi_s = 1 - \theta_0$ (Appendix I)].

This section reviews seven seismic wave velocity models. The time-average, Minshull et al. (1994), weighted equation (Lee et al. 1996), and three-phase models directly calculate the P wave and S wave velocities. The Zimmerman and King (1986) and BGTL models calculate the bulk and shear moduli, which could be used to derive the P and S wave velocities [Eqs. (1) and (2)]. The complete equations for the seismic wave velocity models are presented in Appendix II. Table 1 summarizes the assumptions and applications of these models. Some models are extended from poroelastic theory, which adds assumptions for permafrost [e.g., Zimmerman and King (1986) and three-phase models]. Some models were initially proposed based on other materials, such as rock and gas hydrates [e.g., time-average, Minshull et al. (1994), weighted equation, and BGTL models] and applied in saturated permafrost. The conclusions drawn from hydrate sediment studies should be evaluated before applying them to unconsolidated permafrost, despite the similarities between frozen soil and gas hydrate (Pearson et al. 1983; Lyu et al. 2020).

Table 1. Assumptions and applications of seismic wave velocity models

Models	Assumptions	Applications
Time-average (Wyllie et al. 1958; Timur 1968)	This model assumes rigid consolidated rock with little fluid. The wave velocities and transmission coefficients are independent of frequencies for elastic media when there is no slippage or separation of interfaces	P wave velocity of gas hydrates or permafrost (which uses artificially low matrix velocity for unconsolidated sediments)
Zimmerman and King (1986)	This model assumes discontinuous water phase in frozen soils and only considers spherical shape for water and soil phases of unconsolidated permafrost	Permafrost porosities $\phi \in [0.3, 0.5]$ and low unfrozen water saturation below 60%
Minshull et al. (1994)	This model uses a two end-member mixing approach based on time-average model and Gassmann's equation. Poisson's ratio is independent of porosity	Initially proposed for partially gas-saturated oceanic sediments
Weighted equation (Lee et al. 1996)	This model calculates the weighted average of the three-phase Wood equation and the time-averaged model, and only considers spherical shapes for water and soil phases of unconsolidated permafrost	Initially proposed for unconsolidated gas hydrates
Three-phase (Leclaire et al. 1994)	This model is extended based on Biot theory, the corresponding assumptions are statistically isotropic, fully saturated, and with a uniform and connected porosity. In addition, it assumes no direct contact between solid grains and ice inclusions	Frozen porous media
BGTL theory modified by Lee (Lee 2002)	This model is extended based on Biot theory. The V_p/V_s ratio of a consolidated sediment is related to the V_p/V_s ratio of the matrix material and the effective porosity of the soil	Initially proposed for gas hydrates
Two end-member model (Dou et al. 2017)	This model uses a two end-member mixing approach based on self-consistent approximation and Biot theory	Initially proposed for saturated, unconsolidated saline permafrost

Time-Average Model (Wyllie et al. 1958 and Timur 1968)

The time-average model [Eq. (10)] estimates the effective slowness (i.e., the inverse of velocity) of the multiphase material as the volume-weighted average slowness of the constituents of the two-phase material (Wyllie et al. 1958). The model calculates the average time needed for the P wave velocity to travel through the material. The assumption is that the P wave velocity and the transmission coefficient are independent of the wave frequencies for elastic media when there is no slippage or separation of the interfaces. Timur (1968) first proposed a three-phase, time-average equation to explain the compressional wave velocity in various consolidated rocks that are measured at subzero temperatures. It calculates the sum of the travel time of the individual components and is highly idealized for rock material.

The time-average model is empirical and lacks a physical basis. In applications to saturated permafrost, the time-average model could be considered to assume fully frozen permafrost (Lyu et al. 2020) and predict V_p . In addition, the assumption leads to overestimating the P wave velocity. Therefore, some studies use artificially low P wave velocities of the soil matrix (V_{ps}) (Hoyer et al. 1975; Lee et al. 1996). The model is not applicable if the material is unconsolidated (Wyllie et al. 1958; Dvorkin and Nur 1998), has clay or organic content, or contains secondary porosity such as fractures (Timur 1968; Castagna et al. 1985; Eberhart-Phillips et al. 1989).

Zimmerman and King (1986) Model

Zimmerman and King (1986) extended the two-phase wave-scattering theory of Kuster and Toksöz (1974) for estimating the three-phase bulk and shear moduli of unconsolidated permafrost (King et al. 1988; Zimmerman and King 1986). Because limited parameters are required, the model [Eqs. (11)–(14)] was frequently used (King et al. 1988; Lyu et al. 2020). The Zimmerman and King (1986) model assumes unconsolidated permafrost with spherical soil particles embedded in ice—water mixtures. The ice—water mixture is composed of spherical water inclusions in a continuous ice phase. In addition, the model assumes a discontinuous water phase in the frozen soil; therefore, porosities between 30% and 50% and low unfrozen water saturation below 60% could be estimated. This assumption might be invalid for frozen soils with a high unfrozen water content.

Minshull et al. (1994) Model

The Minshull et al. (1994) model [Eqs. (15)–(20)] employs a dual end-member mixing approach to calculate the seismic wave velocities of permafrost. This model constitutes two end members: (1) fully ice-saturated sediment (completely frozen) as the stiff end member; and (2) fully water-filled sediment (completely unfrozen) as the soft end member. The fully frozen end uses the time-average model, and the fully unfrozen end employs Gassmann's equation (Gassmann 1951). By averaging the two end members, the P and S wave velocities of partially frozen permafrost could be derived.

Weighted Equation Model (Lee et al. 1996)

The weighted equation model [Eq. (22)] that was proposed by Lee et al. (1996) is a modification of the weighted average relationship that was proposed by Nobes et al. (1986). The model calculates the weighted average of the three-phase time-average model (Timur 1968; Wyllie et al. 1958) and Wood equation (Wood 1941) of the P wave velocity, initially proposed for hydrate-bearing sediments (Lee et al. 1996). The S wave velocity (V_s) in the weighted equation model could be approximately predicted based on an empirical equation for mudrock by Castagna et al. (1985) [Eq. (23)]. When applying the weighted equation model to permafrost, this

empirical linear relationship between the P and S wave velocities needs to be revised.

Three-Phase Model (Leclaire et al. 1994)

The three-phase model by Leclaire et al. (1994) [Eqs. (26) and (27)] is an extension of the two-phase Biot theory, which imposes a soil grain-water-ice layered medium structure. Biot theory describes wave propagation in a statistically isotropic, fully saturated medium with uniform porosity (Biot 1956; Lyu et al. 2020). The three-phase model assumes no direct contact between the solid grains and ice (Leclaire et al. 1994). The model considers the influence of potential and kinetic energy and a stress-strain relationship for wave propagation in a frozen medium (Leclaire et al. 1994). Due to the strong theoretical basis, it requires many material properties and empirical factors, such as soil and hydrate matrix permeability, friction coefficients, and the viscosity of free water. These values are difficult or impossible to measure, and some need to be determined by data fitting (Lyu et al. 2020). The three-phase model utilizes the Kuster and Toksöz (1974) equation, which was initially proposed for two-phase media and commonly used for low-porosity rocks to derive the ice matrix elastic moduli.

Lee (2002) modified the Biot-Gassmann theory (Biot 1956; Gassmann 1951) by updating the original two-phase Biot theory; the modified model is the BGTL model [Eqs. (58)-(61)]. This model was proposed for unconsolidated gas hydrate-bearing sediments (Lee 2002). The BGTL model considers the effective solid matrix that consists of soil grains and ice based on the Hashin-Shtrikman (HS) average equation (Hashin and Shtrikman 1963; Hill 1952). In the BGTL model, Lee (2002) assumed that the relationship between the P and S wave velocities between soil and its solid skeleton were proportional to $(1-\phi_w)$ [Eq. (56)] and proposed an empirical relationship between the Biot coefficient (β) and volume proportion of unfrozen water $(\phi_w = \theta_u)$ that used the weighted equation model [Eq. (57)]. The latter assumption [Eq. (57)] is invalid when grains lose contact in high porosity materials. The empirical relationship in Eq. (56) is derived from tested examples of gas hydrate-bearing sediments with ϕ_w in the range of 0.19– 0.68 (Lee 2002). When the BGTL model is applied to permafrost, Eq. (54) could yield an imprecise Biot coefficient (β) .

Dou et al. (2017) Model

The two end-member model by Dou et al. (2017) [Eqs. (61)-(70)] is an effective medium model for saturated, unconsolidated saline permafrost and is an improvement on the Minshull et al. (1994) model. In addition, this model could be applied to nonsaline permafrost with a salinity of zero. The two end members that form the effective medium of partially frozen sediments include an ice-filled, fully frozen end member and a water-filled, fully unfrozen end member (Dou et al. 2017). The Dou et al. (2017) and Minshull et al. (1994) models use the two end-member mixing approach. Instead of using the time-average model for the fully frozen end, as in the Minshull et al. (1994) model, Dou et al. (2017) used an effective medium modeling procedure. The fully frozen end uses the selfconsistent approximation (Berryman 1995), and the fully unfrozen end uses the Herz-Mindlin contact (Mindlin 1949) and Biot theories (Dou et al. 2017). The Dou et al. (2017) model does not require parameter tuning for the mixing proportions and inherently assumes mixed pore-scale ice distributions. However, it overestimates the P wave velocity at moderate to high ice saturations, which indicates that the model might overestimate the role of cementing ice at those saturations. Another limitation is that the Dou et al. (2017) model uses a modified HS average as a mixing strategy, which lacks a physical interpretation.

Statistical Evaluation of Unfrozen Water Content Models and Seismic Wave Velocity Models in Permafrost

This section evaluates the six unfrozen water content models and proposes a modified model based on the Dall'Amico et al. (2011) model (the modified Dall'Amico's model). Then, the modified Dall'Amico's model was used to evaluate the seven seismic wave velocity models. The data that was used to evaluate the models were collected from published laboratory results. For the unfrozen water content models, 61 data sets of unfrozen water content versus temperature were collected with 943 data points from 12 journal and conference publications. For the seismic wave velocity models, 41 data sets of seismic wave velocities were collected (which

included P and S wave velocities) versus temperature with 369 data points from nine journal and conference publications. All data sets were nonsaline saturated or nearly saturated permafrost. All soil samples were unconsolidated. The index properties and testing conditions of the soil samples are listed in Appendixes III and IV.

Statistical Evaluation of Unfrozen Water Content Models in Permafrost

The 61 data sets of volumetric unfrozen water content with various soil types are shown in Fig. 1, which includes clean sand, sand with fines, silt, clay, and organic soil, which are major soil types based on the Unified Soil Classification System (USCS). Soils were

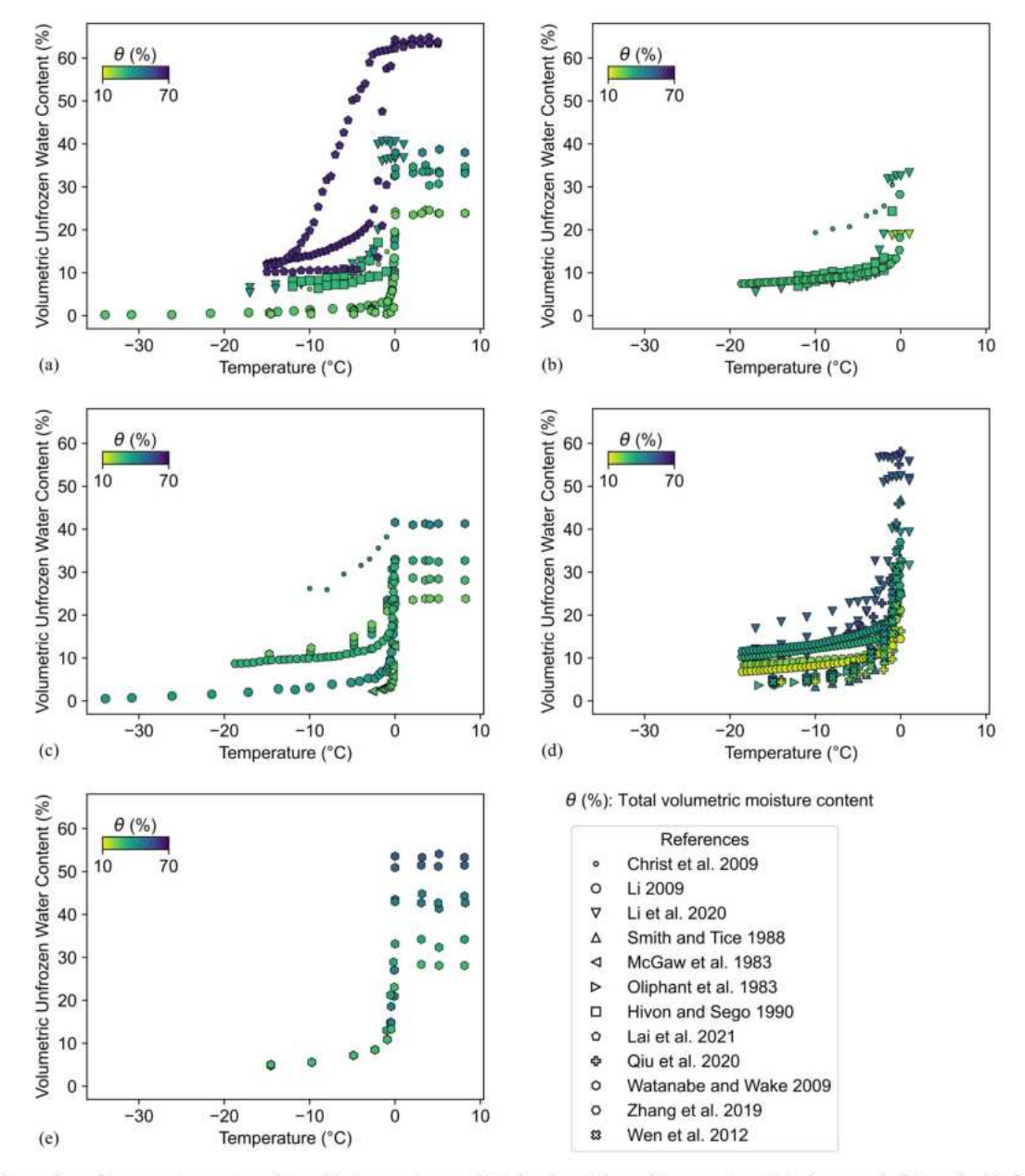


Fig. 1. Volumetric unfrozen water content data with temperature and total volumetric moisture content: (a) clean sand; (b) sand with fines; (c) silt; (d) clay; and (e) organic soil.

classified using the USCS, as listed in Appendix III. More details of the laboratory data can be found in the literature (Christ et al. 2009; Li 2009; Li et al. 2020; Smith and Tice 1988; McGaw et al. 1983; Oliphant et al. 1983; Hivon and Sego 1990; Lai et al. 2021; Qiu et al. 2020; Watanabe and Wake 2009; Zhang et al. 2019; Wen et al. 2012). This meta-analysis indicated that clay (data sets = 25% or 40%) was the most tested soil, followed by clean sand (data sets = 15% or 25%) and silt (data sets = 9% or 15%). Sand with fines and organic soil was the least tested (data sets = 6% or 10%). Clay permafrost was the most tested, which was probably due to its capability to hold more moisture and, therefore, its higher susceptibility to permafrost degradation. As the temperature decreased from 0°C, the rate of unfrozen water content reduction was higher at approximately 0°C and then gradually decreased as the temperature further decreased. The rate of change in the unfrozen water content was much less below -15°C compared with approximately 0°C.

The residual unfrozen water content (i.e., the water that cannot freeze at extremely low temperatures) is usually difficult to measure. The estimated values used in practice are based on empirical relationships. Based on the Dall'Amico et al. (2011) model, a modified model was proposed that assumed that the permafrost was fully saturated; therefore, the soil–water potential energy that is related to the total water content is zero ($\Psi_{w0} = 0$), and the residual unfrozen water content is ignored to simplify the calculation (i.e., $\theta_{res} = 0$)

$$\theta_{u} = \theta_{0} \left\{ 1 + \left[-\beta' \frac{L_{wi}}{gT_{f}} (T - T_{f}) \right]^{n'} \right\}^{-\left(1 - \frac{1}{n'}\right)}$$
 (6)

where β' and n' = fitting parameters.

The modified Dall'Amico's model is a semitheoretical model that is based on soil temperature and assumes that the permafrost is fully saturated and the residual unfrozen water content is zero. The model needs one variable and two fitting parameters, which are simplified for practical purposes. The modified Dall'Amico model [Eq. (6)] was evaluated with the six unfrozen water content models, which used the root mean square error (RMSE) and average deviation. The RMSE is the square root of the average of the squared differences between the predicted and true values in the collected data sets. A lower RMSE value indicates that the model makes better predictions on the data set. The unit of RMSE is the same as the evaluated variable. The average deviation is the mean of the predicted minus the measured values and could quantify whether the models were biased to overestimate or underestimate quantities of interest. Fig. 2 shows the calculated and measured volumetric unfrozen water contents of the 61 soil samples by the six existing models and the modified Dall'Amico model for different soil types that include clean sand, sand with fines, silt, clay, and organic soil. Figs. 7 and 8 show the RMSE values and average deviations of the seven models for the volumetric unfrozen water content data sets that are grouped by soil types.

The regression analysis showed a similar prediction accuracy of the modified Dall'Amico's compared with the original model. The modified model showed slightly larger RMSE values for clean sand and sand with fines than the values of the original model and required fewer input properties (Appendix I). The values that were predicted by the modified Dall'Amico model for clay samples had a smaller RMSE, which indicated a better performance than the Dall'Amico et al. (2011) model for clay. The modified model has the advantages of a sound theoretical basis, good performance, and a suitable amount of input properties. The ranges of the two fitting parameters of the modified Dall'Amico model were derived

based on the fitting results: (1) $\beta' \in (2.49, 3610)$, $n' \in (1.13, 2.72)$. In the following section, the modified Dall'Amico model is used to predict unfrozen water content that is used as an input for the seismic wave velocity models.

The prediction of all unfrozen water content models showed an overall good performance. This was because all the unfrozen water content models that were reviewed and evaluated in this paper use fitting parameters. However, the disadvantage of these models is the determination of fitting parameters when the models are applied to a sample without unfrozen water content measurements. The Anderson and Tice (1972) and Zhang et al. (2017) models are empirical models with simple equations. These models are easy to apply but have less accuracy. The Anderson and Tice (1972) model provides good performance with the advantage of a simple formula format; however, it underestimates θ_u for sand with measured θ_{u} between 30% and 50%. But its prediction approaches infinity when the temperature is approximately 0°C. The Zhang et al. (2017) model was initially proposed for silt and performs well for sand with fines. The performance of the Zhang et al. (2017) model is unsuitable for clean sand, clay, and organic soil. Fig. 2(e) shows a general trend that the Zhang et al. (2017) model overestimates θ_{μ} when the measured θ_{μ} is < 25% and underestimates θ_{μ} as the measured θ_{μ} increased.

The Michalowski (1993), McKenzie et al. (2007), and Kozlowski (2007) models have similar formulas, which use exponential equations and consider residual unfrozen water content. The Kozlowski (2007) model with two fitting parameters performed better than the models that have a similar formula format but one fitting parameter, which includes the Michalowski (1993) and McKenzie et al. (2007) models [Figs. 2(a–c)]. The Michalowski (1993) and McKenzie et al. (2007) models underestimated θ_u for the measured θ_u below 20%. In addition, the Michalowski (1993) model underestimated θ_u for sand with the measured θ_u above 30%. The McKenzie et al. (2007) model overestimated θ_u for sand and clay with the measured θ_u above 30%. The similar performance from the Michalowski (1993) and McKenzie et al. (2007) models might be due to similar formula trends; both use an exponential equation and consider the residual unfrozen water content.

Statistical Evaluation of Existing Seismic Wave Velocity Models in Permafrost

This section evaluates the seven seismic wave velocity models in nonsaline saturated permafrost. Table 2 summarizes the number of data sets and points for each soil type. More details of the laboratory data can be found in Appendix IV and the literature (Wang et al. 2006; Christ et al. 2009; Nakano and Arnold 1973; Kim et al. 2016; Li 2009; Meng et al. 2008; Fu et al. 1983; Yang et al. 2015; Ge et al. 2013; Zhang et al. 2018). All data sets were nonsaline saturated permafrost. The data from the original publications included the P and S wave velocities, bulk, shear, and Young's moduli, and Poisson's ratio. All elastic moduli that were collected were converted into seismic wave velocities based on Eqs. (1)–(4).

The data sets represented the variations in the seismic wave velocities with temperature for various soil types (e.g., clean sand, sand with fines, silt, clay, and organic soil) and are shown in Fig. 3 (P wave velocity versus temperature) and Fig. 9 (S wave velocity versus temperature). As the temperature decreased from 0°C, the increase rates in the P and S wave velocities were higher at approximately 0°C and gradually decreased as the temperature further decreased. This trend was consistent with the decrease rate in the unfrozen water content as the temperature decreased (Fig. 1), which indicated that the variation in the seismic wave velocities was correlated with the variation in the unfrozen water content.

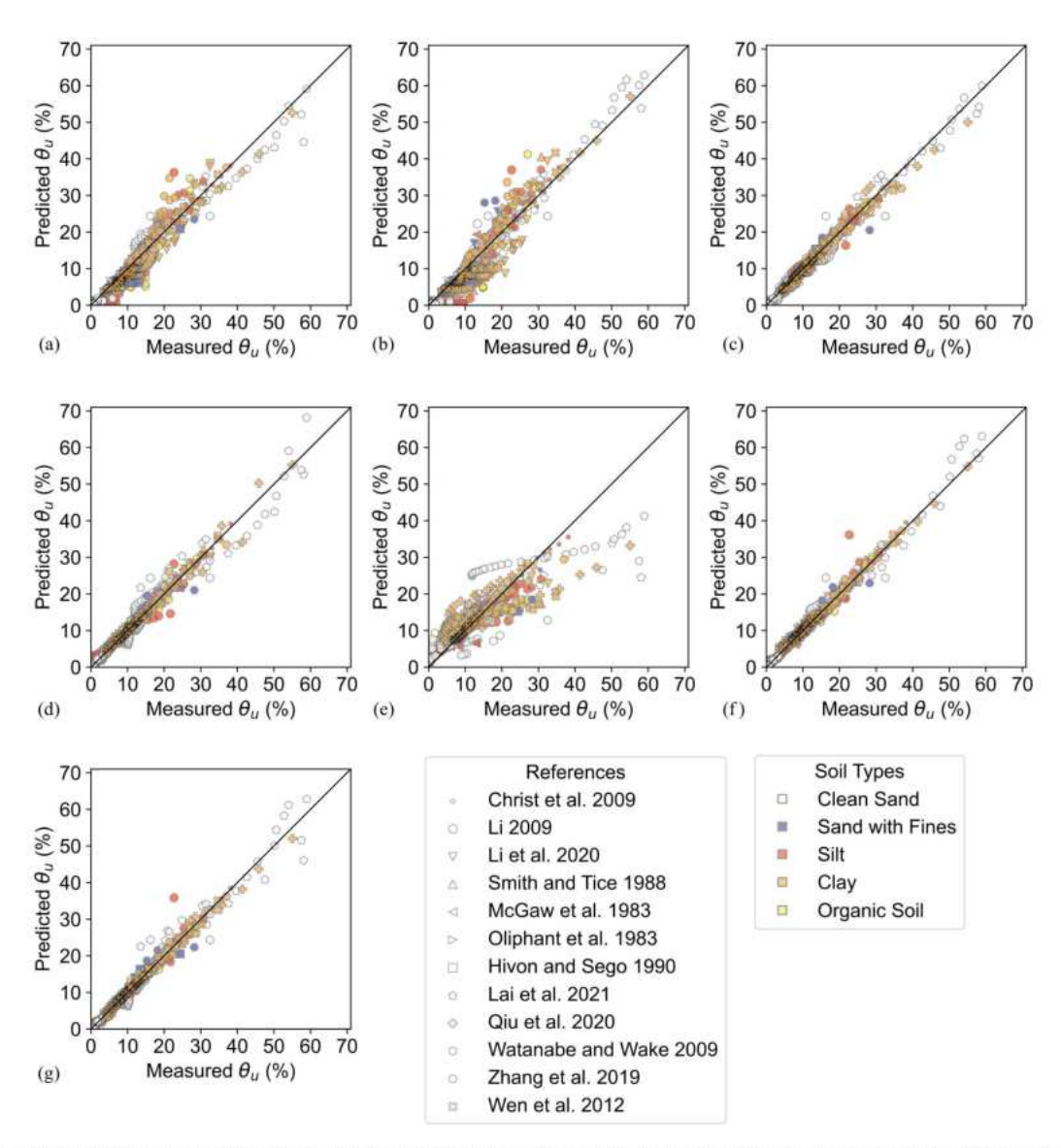


Fig. 2. Comparisons between the measured and calculated volumetric unfrozen water contents of the six current models and the proposed model: (a) Michalowski (1993); (b) McKenzie et al. (2007); (c) Kozlowski (2007); (d) Anderson and Tice (1972); (e) Zhang et al. (2017); (f) Dall'Amico et al. (2011); and (g) modified model (this paper).

Table 2. Number of data sets for seismic wave velocities

Soil types	Number of data sets	Number of data points		
Clean sand	14	111		
Sand with fines	9	103		
Silt	9	73		
Clay	8	48		
Organic soil	1	31		
Total	41	369		

By comparing V_p (Figs. 3) and V_s (Figs. 9) with the temperature of each soil type, similar trends were observed between the P and S wave velocities. Nakano and Arnold (1973) conducted seismic wave velocity experiments for clean sand under various total moisture contents, which are shown in Figs. 3(a) and 9(a). A higher total moisture content corresponded to higher V_p and V_s for clean sand in saturated permafrost (Nakano and Arnold 1973).

The data sets for V_s and V_p in saturated permafrost are shown in Fig. 4; the linear trend shows a correlation between V_s and V_p for saturated nonsaline permafrost, which was similar for all soil types. The following equation shows the linear regression relationship between V_s and V_p in Fig. 4 with $R^2 = 0.88$:

$$V_s = 0.6116V_p - 210.4 \tag{7}$$

Eq. (7) is a new empirical linear relationship between the P and S wave velocities for unconsolidated permafrost that is based on a large amount of data (369 data points for the joint P and S wave velocities), which could be applied in the weighted equation model to calculate V_s , as a replacement for Eq. (23). Because Eq. (23) was derived based on mudrock (Castagna et al. 1985), the replacement by Eq. (7) could increase the accuracy of V_s predictions in the weighted equation model for permafrost.

First, the modified Dall'Amico's model [Eq. (6)] was used to predict the unfrozen water content, which was used as input for

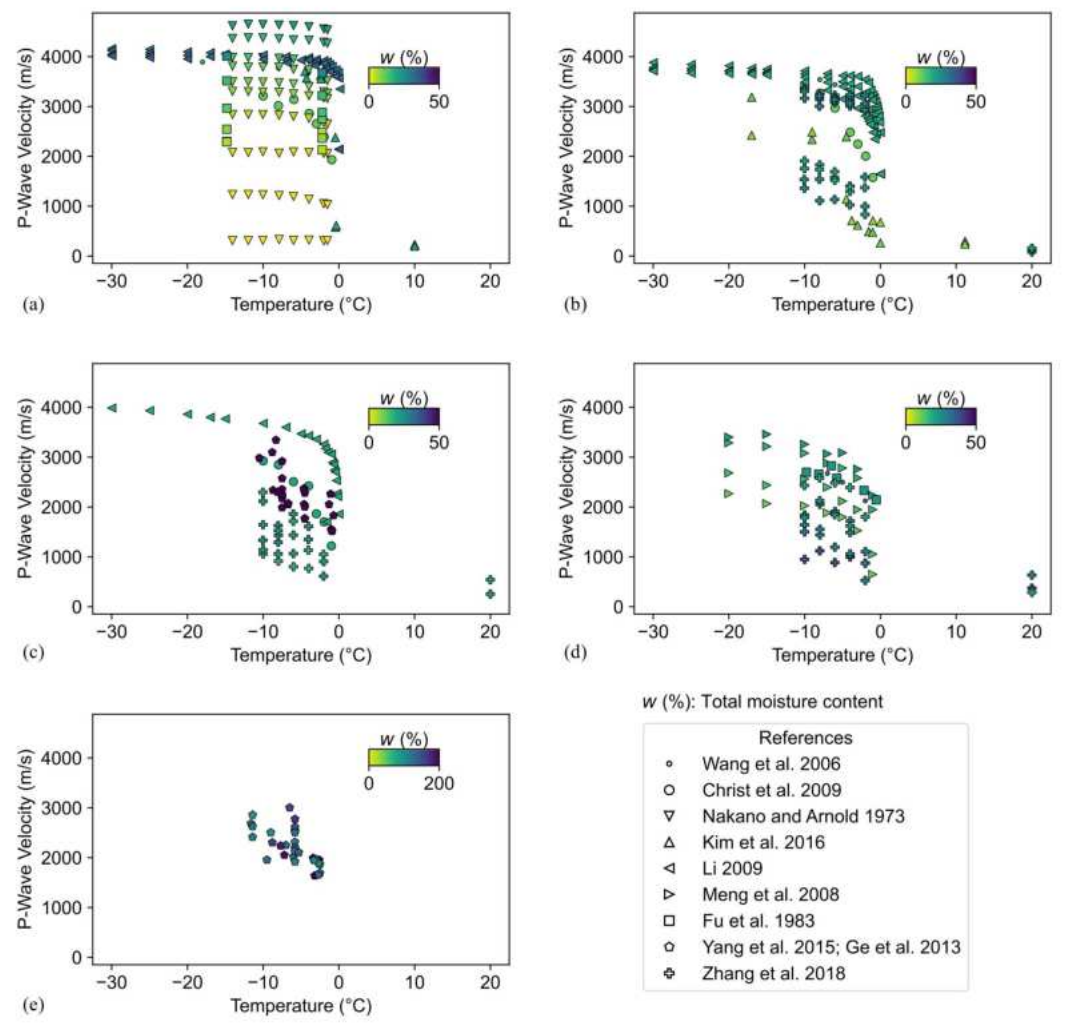


Fig. 3. P wave velocity data of various soils with temperature and total moisture content: (a) clean sand; (b) sand with fines; (c) silt; (d) clay; and (e) organic soil.

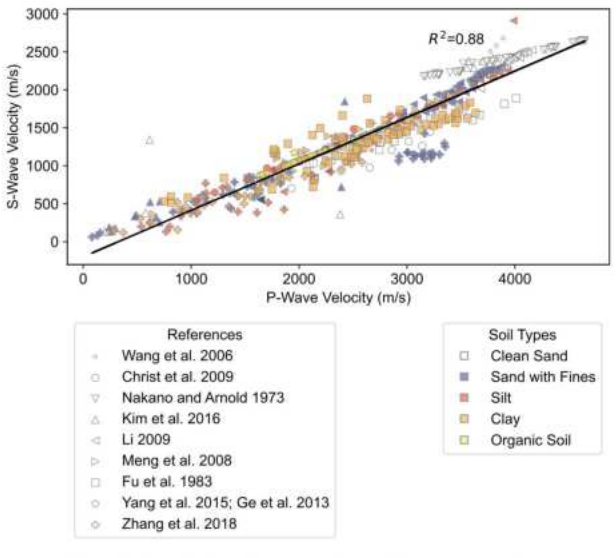


Fig. 4. Correlations between P and S wave velocities.

the seismic wave velocity models. Therefore, the evaluation results could only represent the performance of the seismic wave velocity models that were based on the predicted unfrozen water content, which might introduce uncertainty in the evaluation results. The applied fitting parameter ranges of the modified Dall'Amico's model in this paper are summarized in Table 3 for different soil types, where the β' and n' values were selected to make the best fit of the seismic wave velocity models.

The calculated and measured seismic wave velocities of 41 soil samples are shown in Fig. 5 for the P wave velocities and Fig. 6 for the S wave velocities. The time-average model predicts P wave

Table 3. Parameter ranges of the modified Dall'Amico's model for different soil types

Soil type	$oldsymbol{eta}'$	n'
Clean sand (θ_u <40%)	[6, 100]	[1.7, 2.7]
Clean sand $(\theta_u > 40\%)$	223	1.57
Sand with fines	[2.5,10]	[1.2, 1.8]
Silt	[2.5,5]	[1.2, 1.8]
Clay	[1.2, 2.7]	2.5
Organic soil	4	1.8

velocities. Therefore, it is not shown in Fig. 6. The values that were used for the elastic moduli and densities are given in Table 4. Figs. 12-15 show the RMSE values and average deviations for different models for the P and S wave velocities for different soil types. Of note, the time-average model could only predict V_p with an overestimation. Table 5 summarizes the evaluation results and suggests applications of the seven seismic wave velocity models of saturated permafrost. The seismic wave velocities that were calculated by the Minshull, Dou et al. (2017), and BGTL models matched better with the measured data than other models.

The performance of different models for saturated nonsaline permafrost varied due to the different theories and assumptions. For all soil types, the time-average and weighted equation models mostly overestimated the P wave velocities. The time-average model showed poor predictions among all the models and might be unsuitable for seismic wave velocity predictions in permafrost. In addition, the time-average model cannot predict S wave velocities. For the time-average model, this was due to the assumption that the fully frozen state of permafrost and unfrozen water exist in permafrost. Among the seven seismic wave velocity models, this could be treated as the upper bound prediction.

The performance of the weighted equation model was similar to that of the time-average model because the weighted equation model uses input from the time-average model. In the weighted equation model, Lee et al. (1996) selected W=1 and n=1 to fit the joint P and S wave velocities that were reported by Zimmerman and King (1986). It is challenging to establish the values of W and N for predictions, because the values depend on the observed data (Lee et al. 1996; Lee 2002). Here, W>1 favors the Wood equation [Eq. (19)] (Nobes et al. 1986). In this paper, W=1.1 and N=1 were selected.

The empirical equation of the Biot coefficient (β) [Eq. (57)] in the BGTL model is derived from the weighted equation model, and the performance of the BGTL model is better than the weighted equation model. The weighted equation and BGTL models have acceptable predictions for silt, clay, and organic soils when $V_p < 3,000$ m/s; however, they overestimated V_p and V_s for sand with fines, as shown in Figs. 5(d) and 6(e). In the BGTL model, V_{pc}/V_{sc} (the P and S wave velocities of the porous solid matrix) are assumed to be equal to the multiplication of V_p/V_s and the solid fraction for unconsolidated permafrost [Eq. (56)]; however, the actual V_{pc}/V_{sc} was smaller than the value assumed by the BGTL model.

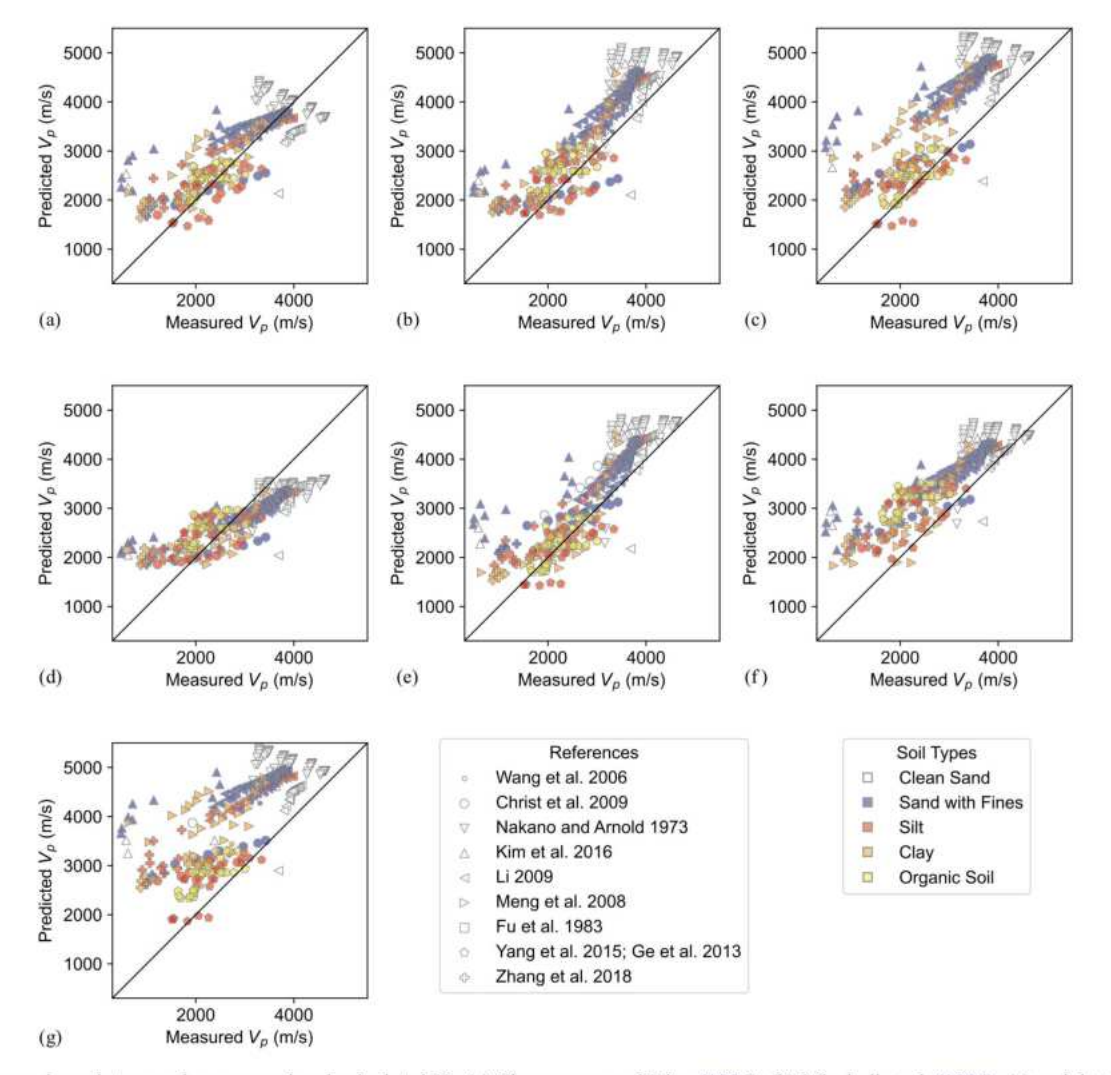


Fig. 5. Comparisons between the measured and calculated V_p : (a) Zimmerman and King (1986); (b) Minshull et al. (1994); (c) weighted equation; (d) three-phase; (e) BGTL; (f) Dou et al. (2017); and (g) time-average models.

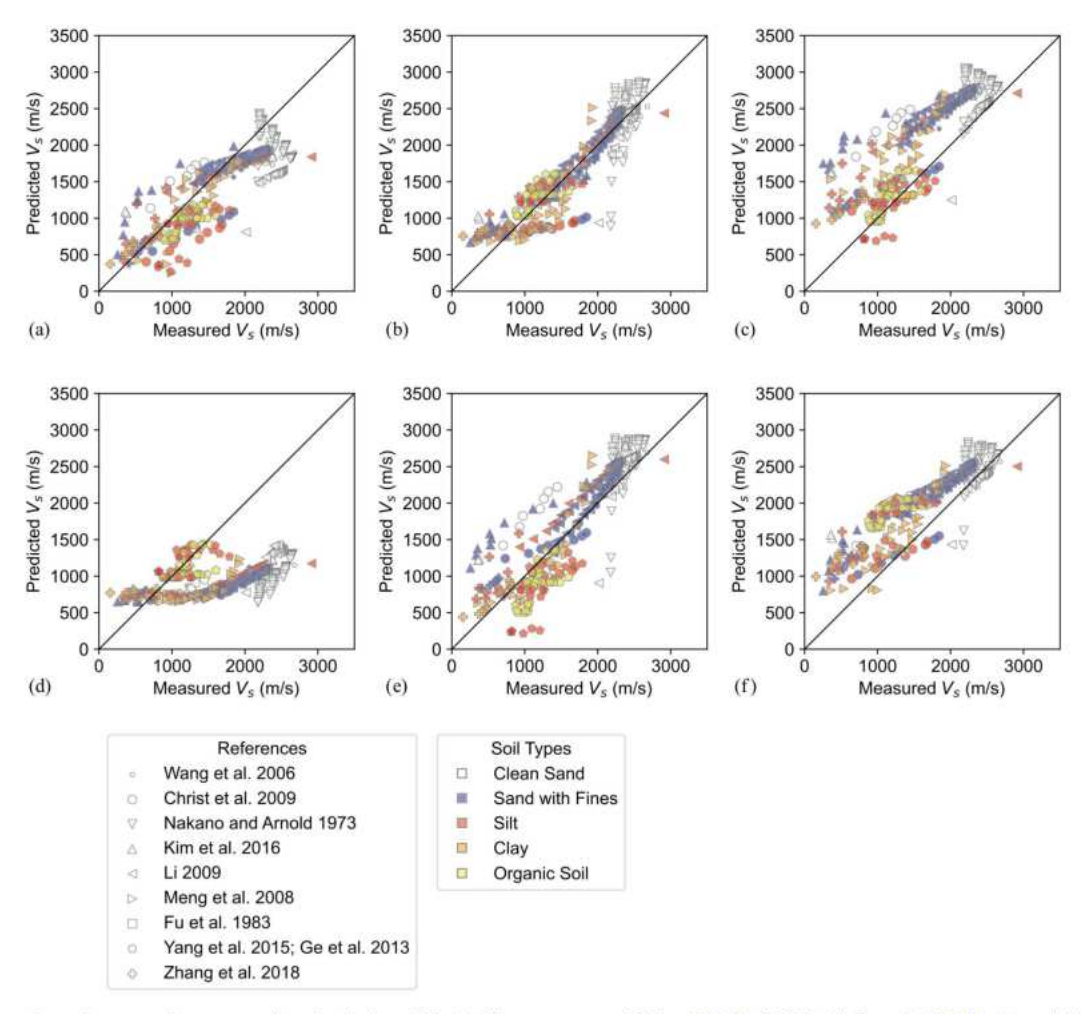


Fig. 6. Comparisons between the measured and calculated V_s : (a) Zimmerman and King (1986); (b) Minshull et al. (1994); (c) weighted equation; (d) three-phase; (e) BGTL; and (f) Dou et al. (2017) models.

Table 4. Elastic moduli and densities of materials

Materials	K (GPa)	G (GPa)	ρ (kg/m ³)
Quartz	44	37	$G_s \cdot \rho_w$
Ice	8.4	3.7	920
Water	2.0	0	1,000
Soil matrix $(K_{sm} \text{ and } G_{sm})$	1	1	_

Therefore, the BGTL model has a relatively low bias but a large prediction error [Figs. 6(e), 13(e), and 15(e)]. Another error source was from the Biot coefficient estimation. When the temperature increased, the S wave velocity that was estimated by the BGTL model was less than the actual measurements for fine-grained soils [Fig. 6(e)].

The Zimmerman and King model generally performs better with decreasing unfrozen water content, which corresponds to higher V_p and V_s values. A trend is shown in Fig. 5(b), especially for sand with fines. This was because the Zimmerman and King model assumes a medium unfrozen water content range (<60%). However, when ice formation starts at approximately 0°C, the water phase might be continuous. Therefore, the Zimmerman and King model might overestimate the seismic wave velocities in most soils as the temperature increases.

The Minshull et al. (1994) model is a two end-member mixing approach, which provided an overall good performance for each soil type. The two end members are mixed to model the intermediate, partially frozen sediment, and the mixing proportions are equal to the relative proportions of the pore ice and water. Instead of relying on parameter tuning, the mixing proportion is consistent over the full range of the possible ice saturations. However, the mixing scheme in Minshull et al. (1994) cannot apply to unconsolidated sediments, because the time-average model [Eq. (10)] is used to model the velocities of the fully frozen end-member and partially frozen condition. Therefore, the Dou et al. (2017) model is an improvement on the Minshull et al. (1994) model.

The prediction of the three-phase model was relatively accurate when V_p was between 2,000 and 3,000 m/s, overestimated when V_p was <2,000 m/s, and underestimated when V_p was larger than 3,000 m/s. This might be due to the assumption of no direct contact between solid grains and ice inclusions. This assumption worked well for negative temperatures of approximately 0°C when permafrost was close to the unfrozen state but not for lower temperatures as the ice content increased, which was probably due to the complex contact between the soil skeleton, unfrozen water, and ice and the effects of the diffuse double layer and different microstructure of ice. The three-phase model performed better for clean sand and sand with fines and overestimated fine-grained soils that

Table 5. Application of seismic wave velocity models of permafrost based on statistical evaluation

Models	Prediction performance	Suggested applications	Limitations
Time-average (Wyllie et al. 1958; Timur 1968)	Overestimates P wave velocities for all soil types	Predict P wave velocity only; fully frozen permafrost	Cannot estimate S wave velocity or partially frozen permafrost
Zimmerman and King (1986)	Good performance on P wave velocity of clay, and S wave velocity of sand	Predict S wave velocity of sand and P wave velocity of clay	Can only estimate permafrost with porosity between 30% and 50% and low unfrozen water content below 60%
Minshull et al. (1994)	Overall good performance on P and S wave velocities of all soil types	Predict P and S wave velocities for sand with fines and clay, P wave velocity of sand, and S wave velocity of silt	The time-average model is a component of this model
Weighted equation (Lee et al. 1996)	Good performance on S wave velocity of silt	Predict S wave velocity of silt	The time-average model is a component of this model
Three-phase (Leclaire et al. 1994)	Good performance on P wave velocity of silt Good performance on S wave velocity of clay	Predict P wave velocity of silt and S wave velocity of clay	Relatively complicated calculation, requiring many material properties and empirical factors
BGTL theory modified by Lee (Lee 2002)	Good performance on P and S wave velocities of sand and clay Good performance on S wave velocity of sand with fines	Predict P wave velocity of sand and clay and S wave velocity of sand with fines	Initially proposed for unconsolidated gas hydrate-bearing sediments, adaptation needed when applied to for permafrost. Unsuitable for high porosity materials
Dou et al. (2017) model	Overall good performance on P and S wave velocities of all soil types	Predict P and S wave velocities of sand and clay	Suitable for saturated, unconsolidated permafrost. Maight overestimate the role of cementing ice

included silt, clay, and organic soil. The overestimation of V_p in the three-phase model when V_p was < 2,000 m/s V_s of the three-phase model was underestimated for clean sand and sand with fines.

The performances of the S wave velocity predictions differed from the P wave velocity predictions due to different estimation methods for V_s , which included calculation of the composite shear modulus (most common), direct theoretical calculation, and empirical relationships between the P and S wave velocities. The Zimmerman and King (1986) and BGTL models calculate the bulk and shear moduli and derive V_p and V_s . The Minshull et al. (1994) and three-phase models calculate V_p and V_s directly; first, the weighted equation model predicts V_p , then it derives V_s based on the empirical relationship between V_p and V_s . Therefore, the V_p prediction results were more reliable in the weighted equation model than the V_s prediction results. The S wave velocity that was derived by the original weighted equation model depends on the empirical V_p and V_s relationship that was developed for mudrock by Castagna et al. (1985) in Eq. (23). This relationship is unsuitable for permafrost. In this paper, a new empirical linear relationship between V_p and V_s was derived for unconsolidated nonsaline permafrost based on a large amount of data (369 data points for the joint P wave and S wave velocities), as shown in Fig. 4 and Eq. (7). Eq. (7) was used for V_s prediction in the weighted equation model to replace the original equation [Eq.

The performance of the same model varied for different soil types. This indicated that different seismic velocity models should be used depending on the permafrost soil types. For the Zimmerman and King model, the prediction for sand with fines showed better accuracy than other soil types. The BGTL model performed better for clean sand compared with other models. For the V_p of silt, the three-phase model showed lower RMSE values, and the Zimmerman and King model showed larger RMSE values. The performance of the models varied for the same soil type. For example, as V_p decreased, the bias of the Dou et al. (2017) model increased. In addition, as shown in Figs. 5 and 6, the predictions for sand with fines for the data set by Kim et al. (2016) were higher compared with other data sets of sand with fines. This was probably because the testing method that was used by Kim et al. (2016) was a resonant column test, different from the other samples' testing method, which might affect the microstructural distribution of pore ice in the sample.

The unfrozen water content and seismic wave velocity data sets were independent. The unfrozen water content in the seismic wave velocity models was estimated using the modified Dall'Amico's model, and errors in this estimation might contribute to the estimation accuracy of the seismic wave velocity models.

Conclusions

This paper presented an evaluation of six unfrozen water content models for permafrost. The regression analyses showed that semi-empirical models gave an overall good performance (average RMSE values were smaller than 5%) when the appropriate fitting parameters were used. The empirical models were easier to apply than the theoretical models but lacked physical meaning. The empirical models with two fitting parameters performed better compared with models with one fitting parameter. A simple semiempirical semitheoretical model was proposed (the modified Dall'Amico's model) to predict the unfrozen water content based on soil temperature. The proposed model gives a good balance between the theoretical basis and engineering practices with accurate fitting results and simplified calculations.

Seven seismic velocity models were further evaluated with temperature variations for saturated nonsaline permafrost. Regardless of soil type, porosity, grain size, and temperature, the saturated nonsaline permafrost generally shared the same linear correlation between the P and S wave velocities. An empirical relationship was derived between the P and S wave velocities of saturated nonsaline permafrost, which was based on a large number of data points. This relationship could provide valuable information for permafrost studies and engineering applications. This paper evaluated the prediction results of seven seismic wave velocity models

based on the predicted unfrozen water content that used the modified Dall'Amico's model. The statistical evaluation results showed that Minshull et al. and BGTL models have an overall better performance in seismic wave velocity prediction, which was reflected by lower RMSE values than other models. The prediction performance of the seismic wave velocity models varied with permafrost soil type. The application of the seismic wave velocity models for saturated nonsaline permafrost was summarized in this paper, which might offer valuable insights into the use of seismic wave velocity models under different scenarios.

Appendix I. Comparison of Existing Unfrozen Water Content Models

Models	Formulas	Assumptions
Michalowski (1993)	$\theta_u = \begin{cases} \theta_{\text{res}} + (\theta_0 - \theta_{\text{res}}) \exp\left[\mu(T - T_f)\right] & T < T_f \\ \theta_0 & T \ge T_f \end{cases}$	Residual unfrozen water content is independent of soil temperature
McKenzie et al. (2007)	$S_{w} = \begin{cases} S_{wres} + (1 - S_{wres}) \exp\left[-\left(\frac{T - T_{f}}{\gamma}\right)^{2}\right] & T < T_{f} \\ S_{0} & T \ge T_{f} \end{cases}$	Residual unfrozen water content is constant
	$\theta_{u} = \begin{cases} \theta_{\text{res}} + (\theta_{0} - \theta_{\text{res}}) \exp\left[-\left(\frac{T - T_{f}}{\gamma}\right)^{2}\right] & T < T_{f} \\ \theta_{0} & T \ge T_{f} \end{cases}$	
Kozlowski (2007)	$\theta_{u} = \begin{cases} \theta_{\text{res}} & T \leq T_{\text{res}} \\ \theta_{\text{res}} + (\theta_{0} - \theta_{\text{res}}) \exp\left[\delta \left(\frac{T_{f} - T}{T - T_{\text{res}}}\right)^{\epsilon}\right] & T_{\text{res}} < T < T_{f} \\ \theta_{0} & T \geq T_{f} \end{cases}$	Water remains in liquid form when the soil temperature is above T_{f} , and the unabsorbed water is all frozen when the soil temperature is below T_{res}
Anderson and Tice (1972)	$W_{u} = \begin{cases} a(-T)^{b} & T < T_{f} \\ W_{0}, & T \ge T_{f} \end{cases}$	Adsorptive force governs the freezing of pore water
	$\theta_u = \begin{cases} a \cdot \rho_d (-T)^b & T < T_f \\ \theta_0 & T \ge T_f \end{cases}$	
	where	
	$\ln a = 0.5519 \ln S + 0.2618$	
	$\ln b = 0.2640 \ln S + 0.3711$	All liquid water in soil would change into ice if the
Zhang et al. (2017)	$\theta_u = \begin{cases} \theta_0 \left[1 - \left(\frac{T_f - T}{T_{k0} + T_f} \right)^{\omega} \right] & -T_{k0} < T < T_f \\ \theta_0 & T \ge T_f \end{cases}$	soil temperature fell below absolute zero (-273.15°C) Assumption: the residual unfrozen water content
Dall'Amico et al. (2011)	$\theta_u = \theta_{\text{res}} + (\theta_0 - \theta_{\text{res}}) \{1 + [-\beta \Psi(T)]^n\}^{-(1-\frac{1}{n})} \Psi(T) = \Psi_{w0} + \frac{L_{wi}}{2T_f} (T - T_f)$	is constant

Note: all fitting parameters are stated in Table 6.

Appendix II. Equations Used in Unfrozen Water Content and Seismic Wave Velocity Models

Table 6 states the parameters that were used in the unfrozen water content models in Appendix I. The relationship between the volumetric unfrozen (θ_u) and gravimetric unfrozen water contents (W_u) is

$$\theta_u = \frac{W_u \rho_d}{\rho_w} \tag{8}$$

where ρ_d = dry density of soil; and ρ_w = density of water.

The soil–water potential energy $[\Psi(T)]$ is calculated based on the following equation (Dall'Amico et al. 2011):

$$\Psi(T) = \Psi_{w0} + \frac{L_{wi}}{gT_f}(T - T_f)$$
 (9)

where Ψ_{w0} = soil–water potential energy related to the total water content and is equal to the soil–water potential divided by $\rho_{l}g$; ρ_{l} = density of liquid; and g = gravitational acceleration. For saturated soil, Ψ_{w0} = 0.

© ASCE 04024021-12 J. Cold Reg. Eng.

Table 6. Parameters used in unfrozen water content models

Model	Parameter	Explanation
Michalowski (1993)	θ_u	Volumetric unfrozen water content
	$ heta_{ m res}$	Residual volumetric unfrozen water content
	T	Temperature (°C)
	T T_f θ_0	Temperature of freezing or initial freezing point of pore water (°C)
	θ_0	Initial volumetric water content at T_f
	μ	Fitting parameter
McKenzie et al. (2007)	S_{w}	Unfrozen water saturation
	$S_{ m wres}$	Residual saturation corresponding to the residual volumetric unfrozen water content
	S_0	Initial water saturation at T_f
	γ	Fitting parameter
Kozlowski (2007)	$T_{ m res}$	Temperature corresponding to $\theta_{\rm res}$
	δ	Fitting parameter
	ϵ	Fitting parameter
Anderson and Tice (1972)	W_{u}	Gravimetric unfrozen water content
	W_0	Initial gravimetric unfrozen water content
	$ ho_d$	Dry density of soil
	S	Specific surface area of soil grains
	a	Fitting parameter
	b	Fitting parameter
Zhang et al. (2017)	T_{k0}	$T_{k0} = 0$ °C
	ω	Fitting parameter
Dall'Amico et al. (2011)	$\Psi(T)$	Soil-water potential energy (m)
	L_{wt}	The latent heat of phase change between ice and water, $L_{wi} = 334 \text{ kJ/kg}$
	β	Fitting parameter (m)
	n	Fitting parameter

The equations that were used in seismic wave velocity models are summarized as follows.

 Three-phase time-average model (Wyllie et al. 1958; Timur 1968)

$$\frac{1}{V_p} = \frac{\phi_w}{V_{pw}} + \frac{\phi_i}{V_{pi}} + \frac{\phi_s}{V_{ps}}$$
 (10)

where V_{pw} , V_{pi} , and $V_{ps} = P$ wave velocities of water, ice, and soil solids, respectively.

2. Zimmerman and King (1986) model

In the Zimmerman and King (1986) model, the Kuster and Toksöz (1974) equations are used for the moduli of an ice-water mixture, given by

$$\frac{K_h}{K_i} = \frac{1 + \left[\frac{4G_i(K_w - K_i)}{(3K_w + 4G_i)K_i} \right] s}{1 - \left[\frac{3(K_w - K_i)}{3K_w + 4G_i} \right] s}$$
(11)

$$\frac{G_h}{G_i} = \frac{(1-s)(9K_w + 8G_i)}{9K_i + 8G_i + s(6K_i + 12G_i)}$$
(12)

where K_h and G_h = bulk and shear moduli of the ice—water mixture, respectively; K_i and G_i = bulk and shear moduli of ice, respectively; K_w = bulk modulus of water; and $s = \phi_w/(1 - \phi_s)$ is the water saturation.

Similarly, the bulk (K) and shear (G) moduli of the soil can be obtained using the Kuster–Toksöz equations

$$\frac{K}{K_h} = \frac{1 + \left[\frac{4G_h(K_s - K_h)}{(3K_s + 4G_h)K_h} \right] \phi_s}{1 - \left[\frac{3(K_s - K_h)}{3K_s + 4G_h} \right] \phi_s}$$
(13)

$$\frac{G}{G_h} = \frac{(6K_h + 12G_h)G_s + (9K_h + 8G_h)[(1 - \phi_s)G_h + \phi_sG_s]}{(9K_h + 8G_h)G_h + (6K_h + 12G_h)[(1 - \phi_s)\mu G_s + \phi_sG_h]}$$
(14)

where K_s and G_s = bulk and shear moduli of soil solids, respectively.

3. Minshull et al. (1994) model

In the Minshull et al. (1994) model, the P and S wave velocities of the fully frozen end (i.e., V_{pt} and V_{st}) are determined first

$$\frac{1}{V_{pt}} = \frac{(1 - \phi_s)}{V_{pi}} + \frac{\phi_s}{V_{ps}}$$
 (15)

$$\frac{1}{V_{st}} = \frac{(1 - \phi_s)}{V_{si}} + \frac{\phi_s}{V_{ss}}$$
 (16)

where V_{si} and $V_{ss} = S$ wave velocities of ice and soil solids, respectively. The corresponding density is $\rho_t = (1 - \phi_s)\rho_i + \phi_s\rho_s$.

Then, Gassmann's equation is applied to determine the moduli for the fully unfrozen end

$$K_g - K_{sm} = \frac{\left(1 - \frac{K_{sm}}{K_s}\right)^2}{\frac{1 - \phi_s}{K_w} + \frac{\phi_s}{K_s} + \frac{K_{sm}}{K_s^2}}$$
(17)

$$G_g = \mu_{sm} \tag{18}$$

where K_g and G_g = bulk and shear moduli of the water-filled sediment, respectively; K_{sm} and μ_{sm} = bulk and shear moduli of the porous soil matrix, respectively; and K_s and K_w = bulk moduli of soil solids and water, respectively. The density of the water-filled sediment is $\rho_g = (1 - \phi_s)\rho_w + \phi_s\rho_s$.

Finally, the P and S wave velocities of permafrost are obtained by a weighted average of the slowness of the fully frozen end and fully unfrozen end, which uses the unfrozen water saturation (s) as the mixing ratio

$$\frac{1}{V_p} = \frac{(1-s)}{V_{pt}} + \frac{s}{V_{pg}} \tag{19}$$

$$\frac{1}{V_s} = \frac{(1-s)}{V_{st}} + \frac{s}{V_{sg}} \tag{20}$$

where V_{pg} and $V_{sg} = P$ and S wave velocities of the water-filled sediment, which correspond to K_g and G_g in Eqs. (17) and (18).

4. Weighted equation model (Lee et al. 1996)

The weighted equation model (Lee et al. 1996) calculates the weighted average of the P wave velocity based on the three-phase time-average model in Eq. (23) and the Wood equation. The Wood equation calculates the weighted sum of the kinetic energy for the constituents of water, ice, and soil solids (Lee et al. 1996; Lyu et al. 2020)

$$\frac{1}{\rho V_{pa}^2} = \frac{\phi_w}{\rho_w V_{pw}^2} + \frac{\phi_i}{\rho_i V_{pi}^2} + \frac{\phi_s}{\rho_s V_{ps}^2}$$
(21)

where V_{pa} = predicted P wave velocity; and V_{pw} , V_{pi} , and V_{ps} = P wave velocities of water, ice, and soil solids, respectively.

The weighted equation model by Lee et al. (1996) is

$$\frac{1}{V_p} = \frac{W\phi \cdot s^n}{V_{pa}} + \frac{1 - W\phi \cdot s^n}{V_{pb}} \tag{22}$$

where $V_{pb} = P$ wave velocity by the time-average equation [Eq. (23)]; $\phi = \phi_w + \phi_i = \text{porosity}$; unfrozen water saturation $s = \phi_w/\phi$; and W = dimensionless weighting factor. For permafrost, n is a dimensionless constant that simulates the rate of water freezing. An increase in n indicates that the changing rate is faster when freezing.

The S wave velocity (V_s) in the weighted equation model can be approximately predicted based on an empirical equation for mudrock by Castagna et al. (1985)

$$V_s = 0.8621V_p - 1172.4 \tag{23}$$

5. Three-phase model (Leclaire et al. 1994)

The resulting equation to calculate the P wave velocity (V_{pj}) is

$$V_{pj} = \left[\text{Re}(\sqrt{\Lambda_j}) \right]^{-1}, \ j = 1, 2, 3$$
 (24)

where Re = real part; and Λ_j is obtained from the following characteristic equation:

$$A\Lambda^{3} - [\rho_{11}B + \rho_{22}C + \rho_{33}D - 2(R_{11}R_{23}\rho_{23} + R_{33}R_{12}\rho_{12})]\Lambda^{2} + [bR_{11} + cR_{22} + dR_{33} - 2(\rho_{11}\rho_{23}R_{23} + \rho_{33}\rho_{12}R_{12})]\Lambda - a = 0$$
(25)

The coefficients in Eq. (25) are given in Eqs. (28)–(41). The S wave velocity (V_{sj}) is given by

$$V_{sj} = \left[\text{Re}(\sqrt{\Omega_j}) \right]^{-1}, \ j = 1, 2$$
 (26)

where Ω_j is obtained from the second-order equation

$$\Omega^2 \rho_{22} \mu_1 \mu_3 - \Omega(\mu_1 b + \mu_3 d) + a = 0 \tag{27}$$

where V_{pj} and V_{sj} = solutions of Eqs. (24) and (26). The coefficients in Eq. (27) are given in Eqs. (39) and (42)–(47).

The coefficients of Eqs. (25) and (27) are provided in Eqs. (28)–(55). The completed procedures and equations are found in Leclaire et al. (1994)

$$A = R_{11}R_{22}R_{33} - R_{23}^2R_{11} - R_{12}^2R_{33}$$
 (28)

$$B = R_{22}R_{33} - R_{23}^2 (29)$$

$$C = R_{11}R_{33} \tag{30}$$

$$D = R_{11}R_{22} - R_{12}^2 (31)$$

$$R_{11} = [(1 - c_1)\phi_s]^2 K_{av} + K_{sm}$$
 (32)

$$R_{12} = [(1 - c_1)\phi_s]\phi_w K_{av}$$
 (33)

$$R_{22} = \phi_w^2 K_{av}$$
(34)

$$R_{23} = [(1 - c_1)\phi_i]\phi_w K_{av}$$
 (35)

$$R_{33} = [(1 - c_3)\phi_s]^2 K_{av} + K_{im}$$
 (36)

$$\rho_{11} = \phi_s \rho_s + (a_{12} - 1)\phi_w \rho_w \tag{37}$$

$$\rho_{12} = -(a_{12} - 1)\phi_w \rho_w \tag{38}$$

$$\rho_{22} = (a_{12} + a_{23} - 1)\phi_w \rho_w \tag{39}$$

$$\rho_{23} = -(a_{23} - 1)\phi_w \rho_w \tag{40}$$

$$\rho_{33} = \phi_i \rho_i + (a_{23} - 1)\phi_w \rho_w \tag{41}$$

$$a = \rho_{11}\rho_{22}\rho_{33} - \rho_{23}^2\rho_{11} - \rho_{12}^2\rho_{33}$$
 (42)

$$b = \rho_{22}\rho_{33} - \rho_{23}^2 \tag{43}$$

$$c = \rho_{11}\rho_{33} \tag{44}$$

$$d = \rho_{11}\rho_{22} - \rho_{12}^2 \tag{45}$$

$$\mu_1 = [(1 - g_1)\phi_s]^2 \mu_{av} + \mu_{sm} \tag{46}$$

$$\mu_3 = [(1 - g_3)\phi_i]^2 \mu_{av} + \mu_{im} \tag{47}$$

$$b_1 = \eta_D \frac{\phi_w^2}{\kappa_s} \tag{48}$$

$$b_2 = \eta_D \frac{\phi_w^2}{\kappa_i} \tag{49}$$

$$\kappa_s = \frac{\kappa_{s0}\phi_w^3}{(1-\phi_s)^3} \tag{50}$$

$$\kappa_{i} = \frac{\kappa_{i0} \left[\frac{1 - \phi_{s}}{\phi_{i}} \right]^{3}}{\left(\frac{\phi_{w}}{\phi_{b}} \right)^{3}} \tag{51}$$

The tortuosity values

$$a_{12} = \frac{r_{12}(\phi_s \rho)}{\phi_w \rho_w} + 1 \tag{52}$$

$$a_{23} = \frac{r_{23}(\phi_s \rho')}{\phi_w \rho_w} + 1 \tag{53}$$

$$\rho = \frac{\phi_w \rho_w + \phi_i \rho_i}{\phi_w + \phi_i} \tag{54}$$

$$\rho' = \frac{\phi_w \rho_w + \phi_s \rho_s}{\phi_w + \phi_s} \tag{55}$$

6. BGTL model (Lee 2002)

In the BGTL model, Lee (2002) assumed the relationship between the P and S wave velocities between soil and its solid skeleton as

$$\frac{V_{pc}}{V_{ec}} = \frac{V_p}{V_e} (1 - \phi_w)$$
 (56)

where V_{pc} and V_{sc} = P and S wave velocities of the porous solid matrix (soil grains and ice), respectively.

Lee (2002) proposed an empirical relationship between the Biot coefficient (β) and volume proportion of unfrozen water ($\phi_w = \theta_u$) that used the weighted equation model

$$\beta = \frac{-184.0468}{1 + e^{\frac{\phi_w + 0.56468}{0.10817}}} + 0.99494 \tag{57}$$

Then, the Biot coefficient is used to calculate the modulus (M), which describes the pressure that is needed to change the fluid volume without changing the total volume based on Gassmann's theory

$$\frac{1}{M} = \frac{\beta - \phi_w}{K_w} + \frac{\phi_w}{K_w} \tag{58}$$

where K_{sc} = HS average bulk modulus of the solid matrix (soil grains and ice); and G_{sc} = corresponding shear modulus.

The bulk modulus (K) can be calculated as follows:

$$K = K_{sc}(1 - \beta) + \beta^2 M \tag{59}$$

The shear modulus (G) can be estimated from Eqs. (55) and (58):

$$G = \frac{G_{sc}K_{sc}(1-\beta)(1-\phi_w)^2 + G_{sc}\beta^2M(1-\phi_w)^2}{K_{sc} + \frac{4G_{sc}[1-(1-\phi_w)^2]}{3}}$$
(60)

7. Dou et al. (2017) model

The two end-member model by Dou et al. (2017) uses the self-consistent approximation (Berryman 1995), Herz–Mindlin contact (Mindlin 1949) and Biot theories (Dou et al. 2017). The fully frozen end consists of soil grains and ice, which is calculated by self-consistent approximation. The effective moduli of the fully frozen end member ($K_{\rm IF}$ and $G_{\rm IF}$) are calculated from the following

equations:

$$\phi(K_i - K_{IF})P_{*_i}^{\text{penny}} + (1 - \phi)(K_s - K_{IF})P_{*_s}^{\text{sphere}} = 0$$
 (61)

$$\phi(G_i - G_{IF})Q_{*_i}^{\text{penny}} + (1 - \phi)(G_s - G_{IF})Q_{*_s}^{\text{sphere}} = 0$$
 (62)

where P_{*i}^{penny} , Q_{*i}^{penny} , P_{*s}^{sphere} , and Q_{*s}^{sphere} = shape factors calculated based on the bulk and shear moduli (unitless) (Dou et al. 2017).

The fully unfrozen end consists of soil grains and water. First, the effective moduli of the dry granular frame $(K_{sf}$ and $G_{sf})$ are calculated using the Hertz–Mindlin contact theory. Then, the effective moduli of the water-filled granular pack $(K_{WF}$ and $G_{WF})$ are calculated by

$$K_{\rm WF} = \left(V_{P\infty}^2 - \frac{4}{3}V_{S\infty}^2\right)\rho_{\rm WF}$$
 (63)

$$G_{WF} = V_{Soo}^2 \rho_{WF} \tag{64}$$

where $\rho_{WF} = \rho_s(1 - \phi) + \rho_w \phi$; and $V_{P\infty}$ and $V_{S\infty} =$ high-frequency limiting velocities given by Biot's fluid substitution equations (Dou et al. 2017).

The effective moduli of permafrost are calculated based on the modified HS averages as

$$K = \frac{1}{2}(K_{\text{HS}+} + K_{\text{HS}-}) \tag{65}$$

$$G = \frac{1}{2}(G_{\text{HS}+} + G_{\text{HS}-}) \tag{66}$$

$$K_{\text{HS+}} = K_{\text{IF}} + \frac{s}{(K_{\text{WF}} - K_{\text{IF}})^{-1} + (1 - s) \left(K_{\text{IF}} + \frac{4}{3}G_{\text{IF}}\right)^{-1}}$$
(67)

$$G_{\text{HS+}} = G_{\text{IF}} + \frac{s}{(G_{\text{WF}} - G_{\text{IF}})^{-1} + 2(1 - s) \left(\frac{K_{\text{IF}} + 2G_{\text{IF}}}{5G_{\text{IF}} \left(K_{\text{IF}} + \frac{4}{3}G_{\text{IF}}\right)}\right)}$$
(68)

$$K_{\text{HS}-} = K_{\text{WF}} + \frac{1 - s}{(K_{\text{IF}} - K_{\text{WF}})^{-1} + s \left(K_{\text{WF}} + \frac{4}{3}G_{\text{WF}}\right)^{-1}}$$
(69)

$$G_{\text{HS-}} = G_{\text{WF}} + \frac{1 - s}{(G_{\text{IF}} - G_{\text{WF}})^{-1} + 2s \left(\frac{K_{\text{WF}} + 2G_{\text{WF}}}{5G_{\text{WF}} \left(K_{\text{WF}} + \frac{4}{3}G_{\text{WF}}\right)}\right)}$$
(70)

The complete procedures and equations are in Dou et al. (2017).

Appendix III. Index Properties and Testing Conditions for Soil Samples in Unfrozen Water Content Data Sets

References	Test method	Soil types in figures	USCS or soil description if USCS is not available	Total moisture content (%)	Porosity
Christ et al. (2009)	Time domain reflectometry	Clean sand	SP	12	0.28
	5.	Sand with fines	SC	12	0.27
		Silt	ML	20	0.38

(Continued.)

References	Test method	Soil types in figures	USCS or soil description if USCS is not available	Total moisture content (%)	Porosity
Li (2009)	Frequency domain reflectometry sensor; 50 MHz	Silt	ML	20, 26	0.43, 0.49
Li et al. (2020)	Pulsed nuclear magnetic resonance	Clean sand	Medium sand	23, 27	0.41, 0.45
.71 - 53		Sand with fines	Silty clay	20-38	0.45-0.51
		Clay	CL	20-38	0.42-0.46
Smith and Tice (1988)	Nuclear magnetic resonance	Clay	CL	33	0.47
McGaw et al. (1983)	Nuclear magnetic resonance	Silt	Silt	15, 18	0.36
Oliphant et al. (1983)	Nuclear magnetic resonance	Clay	Clay	22	0.46
Hivon and Sego (1990)	Time domain reflectometry	Clean sand	S	17.6	
30.70.5		Sand with fines	SM	16.5	
Lai et al. (2021)	Nuclear magnetic resonance	Clean sand	S	39	_
Qiu et al. (2020)	Collected from literature	Clay	CL	10-32	0.34-0.42
Watanabe and Wake	Nuclear magnetic resonance	Clean sand	S	16-29	_
(2009)	TO CALL PROCESSION AND VICE ADDRESSED ON THE STATE AND APPROXIMENT OF THE STATE AND APPROXIMENT OF THE STATE	Silt	ML	21-37	
		Organic soil	OL	27-51	
Zhang et al. (2019)	Nuclear magnetic resonance	Sand with Fines	SM	17	0.35
		Silt	ML	18	0.38
		Clay	CL	9-23	0.38-0.40
Wen et al. (2012)	Nuclear magnetic resonance	Clay	Silty Clay	16-29	_

Note: USCS = Unified soil classification system.

Appendix IV. Index Properties and Testing Conditions for Soil Samples in Seismic Wave Velocity Data Sets

References	Test method	Soil types in figures	USCS or soil description if USCS is not available	Total moisture content (%)	Porosity	Confining pressure (kPa
Wang et al. (2006)	Ultrasonic; 500 kHz	Clean sand	Fine sand	18	0.38	0
		Sand with fines	SC	19	0.41	
		Fine-grained soil	CL	31	0.45	
Christ et al. (2009)	Ultrasonic; 2 MHz	Clean sand	SP	12	0.28	0
		Sand with fines	SC	12	0.27	
		Fine-grained soil	ML	20	0.38	
Nakano and Arnold (1973)	Ultrasonic; 1 MHz	Clean sand	Medium sand	8-22	0.39-0.41	0
Zimmerman and King (1986)	Ultrasonic; 500- 850 kHz	Clean sand	S	0-5	0.36-0.40	350
		Fine-grained soil	ML-CL, CL	6-22	0.32-0.44	
Kim et al. (2016)	Resonant column	Clean sand	Fine to medium sand	19-21	0.36-0.38	0
		Sand with fines	SC-SM	8-11	0.26-0.27	
Li (2009)	Ultrasonic; 400 kHz	Clean sand	Fine sand	30-34	0.44-0.47	0
		Sand with fines	SC	20	0.50-0.53	
		Fine-grained soil	ML, silt	20-36	0.43-0.49	
King et al. (1988)	Ultrasonic	Clean sand	S	22, 25	0.37, 0.40	340
		Fine-grained soil	C, M	22-29	0.36-0.43	
Meng et al. (2008)	Ultrasonie; 50 kHz	Fine-grained soil	CL	11-22	0.43	0
Fu et al. (1983)	Ultrasonic	Clean sand	Medium sand	5-25	N/A	50
		Fine-grained soil	C			
Yang et al. (2015);	Universal testing machine	Fine-grained soil	ML	62-141	0.63-0.79	0
Ge et al. (2013)		Organic soil	OL	86-225	0.67 - 0.87	
Zhang et al. (2018)		Sand with Fines	SM	26	0.46	0
		Silt	ML	21-26	0.40 - 0.46	
		Clay	CL	24	0.42	

Appendix V. Additional Statistical Evaluation and Analysis Results for Unfrozen Water Content Models and Seismic Wave Velocity Models

This appendix contains additional statistical evaluation and analysis results for the unfrozen water content and seismic wave velocity

models. Figs. 7 and 8 show the RMSE and average deviations for the unfrozen water content models for different soil types. Figs. 9–

© ASCE 04024021-16 J. Cold Reg. Eng.

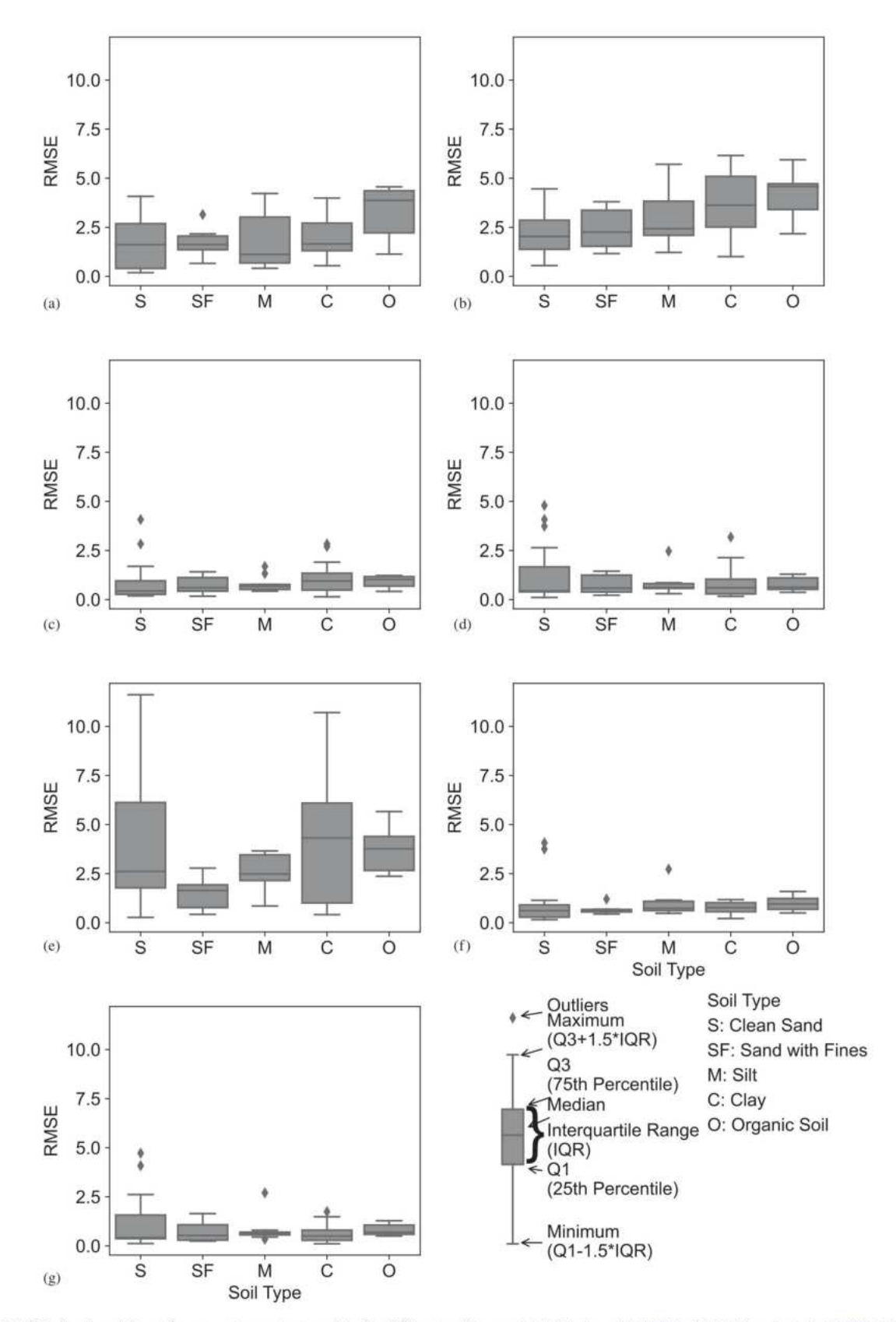


Fig. 7. RMSE of volumetric unfrozen water content models for different soil types: (a) Michalowski (1993); (b) McKenzie et al. (2007); (c) Kozlowski (2007); (d) Anderson and Tice (1972); (e) Zhang et al. (2017); (f) Dall'Amico et al. (2011); and (g) modified (this paper).

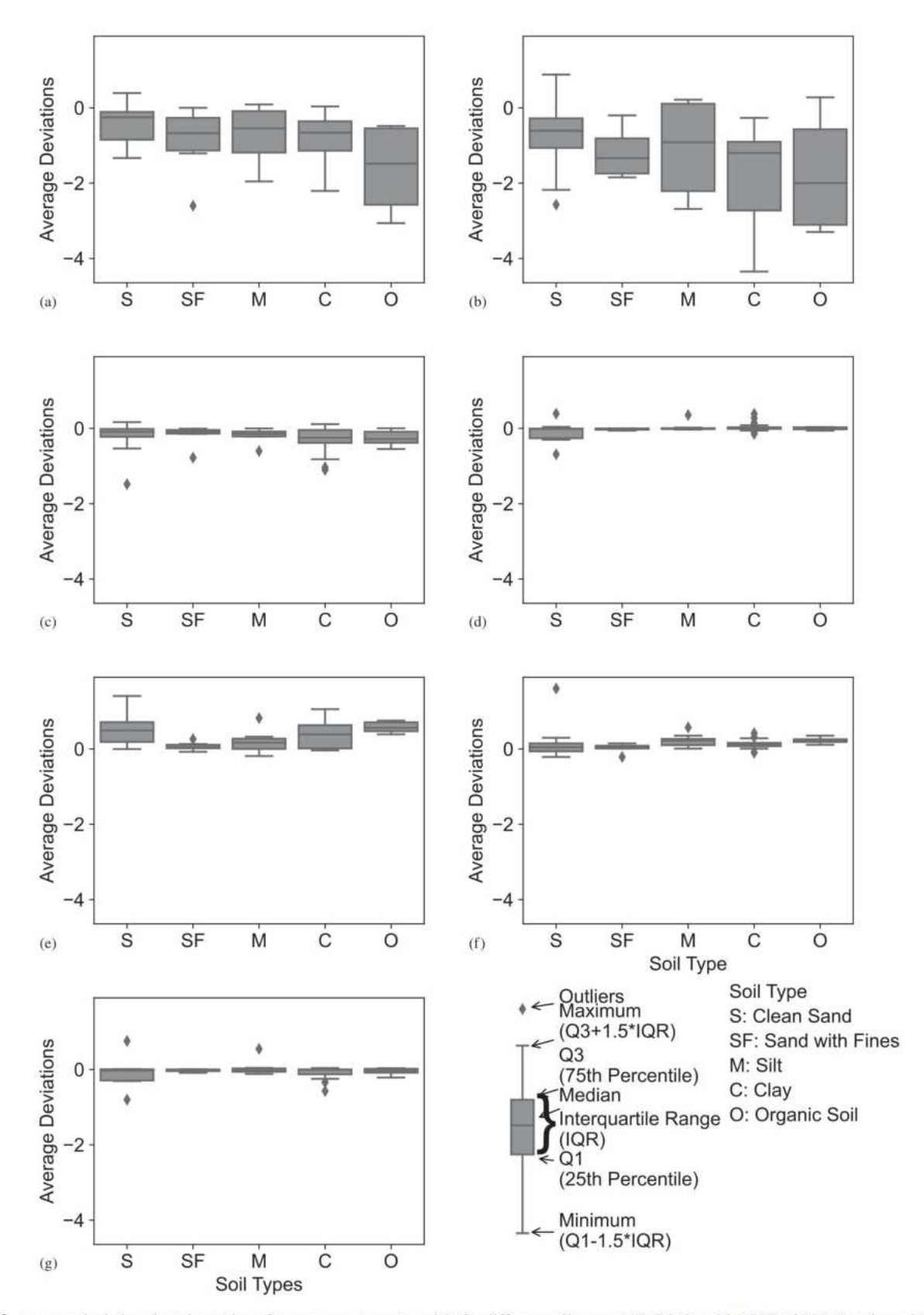


Fig. 8. Average deviations in volumetric unfrozen water content models for different soil types: (a) Michalowski (1993); (b) McKenzie et al. (2007); (c) Kozlowski (2007); (d) Anderson and Tice (1972); (e) Zhang et al. (2017); (f) Dall'Amico et al. (2011); and (g) modified models (this paper)

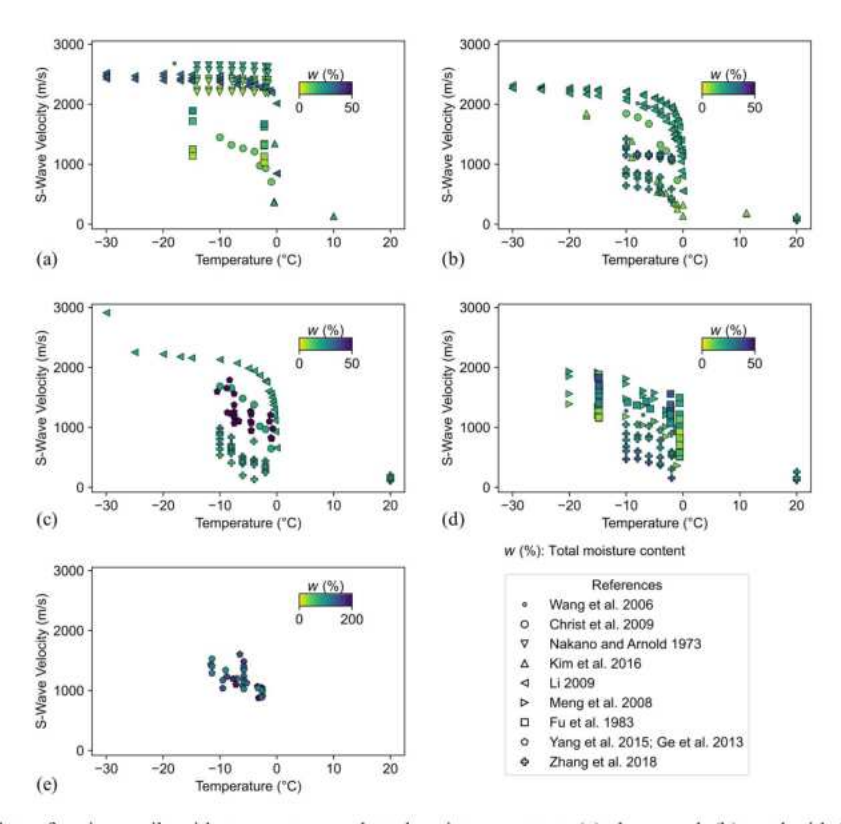


Fig. 9. S wave velocity data of various soils with temperature and total moisture content: (a) clean sand; (b) sand with fines; (c) silt; (d) clay; and (e) organic soil.

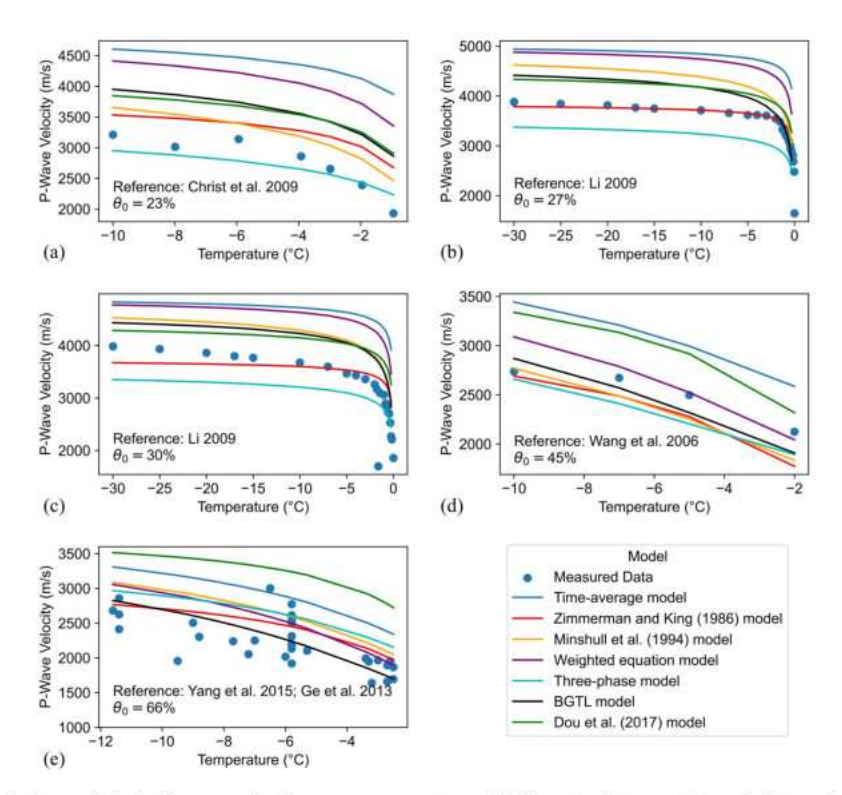


Fig. 10. Seismic wave velocity models for P wave velocity versus temperature of different soil types: (a) sand; (b) sand with fines; (c) silt; (d) clay; and (e) organic soil.

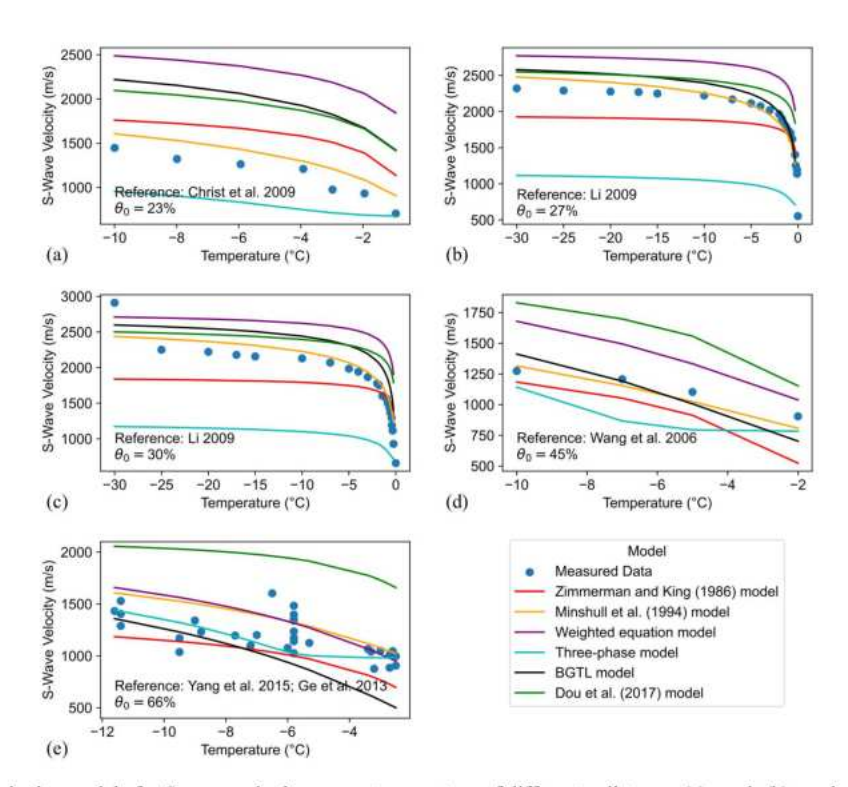


Fig. 11. Seismic wave velocity models for S wave velocity versus temperature of different soil types: (a) sand; (b) sand with fines; (c) silt; (d) clay; and (e) organic soil.

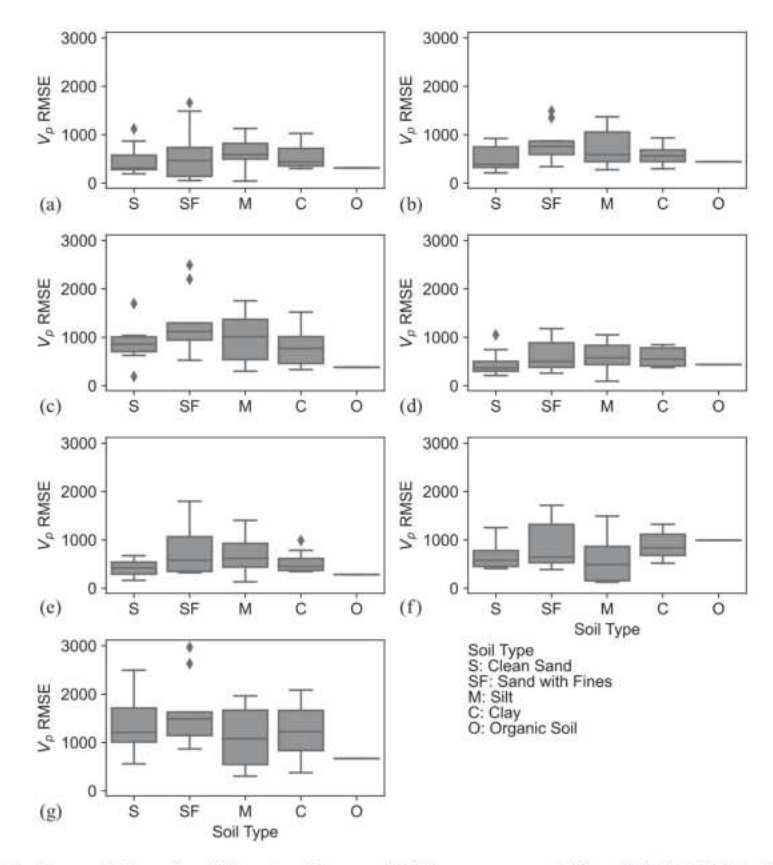


Fig. 12. RMSE of P wave velocity predictions for different soil types: (a) Zimmerman and King (1986); (b) Minshull et al. (1994); (c) weighted equation; (d) three-phase; (e) BGTL; (f) Dou et al. (2017); and (g) time-average models.

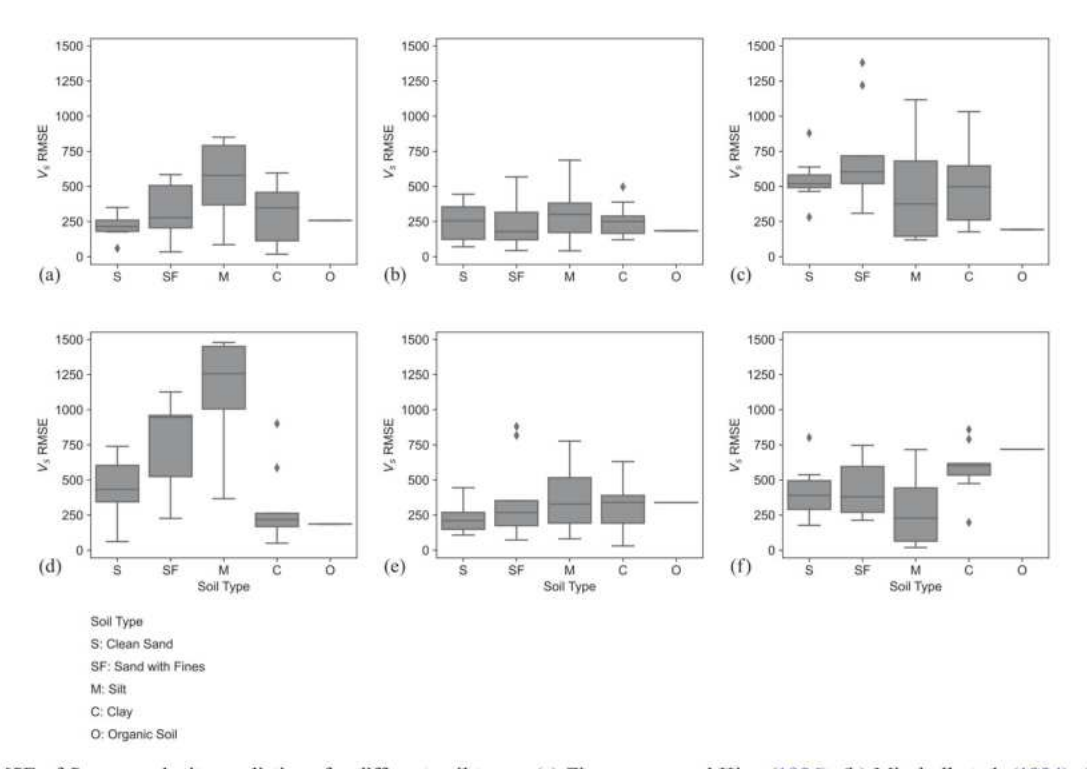


Fig. 13. RMSE of S wave velocity predictions for different soil types: (a) Zimmerman and King (1986); (b) Minshull et al. (1994); (c) weighted equation; (d) three-phase; (e) BGTL; and (f) Dou et al. (2017) models.

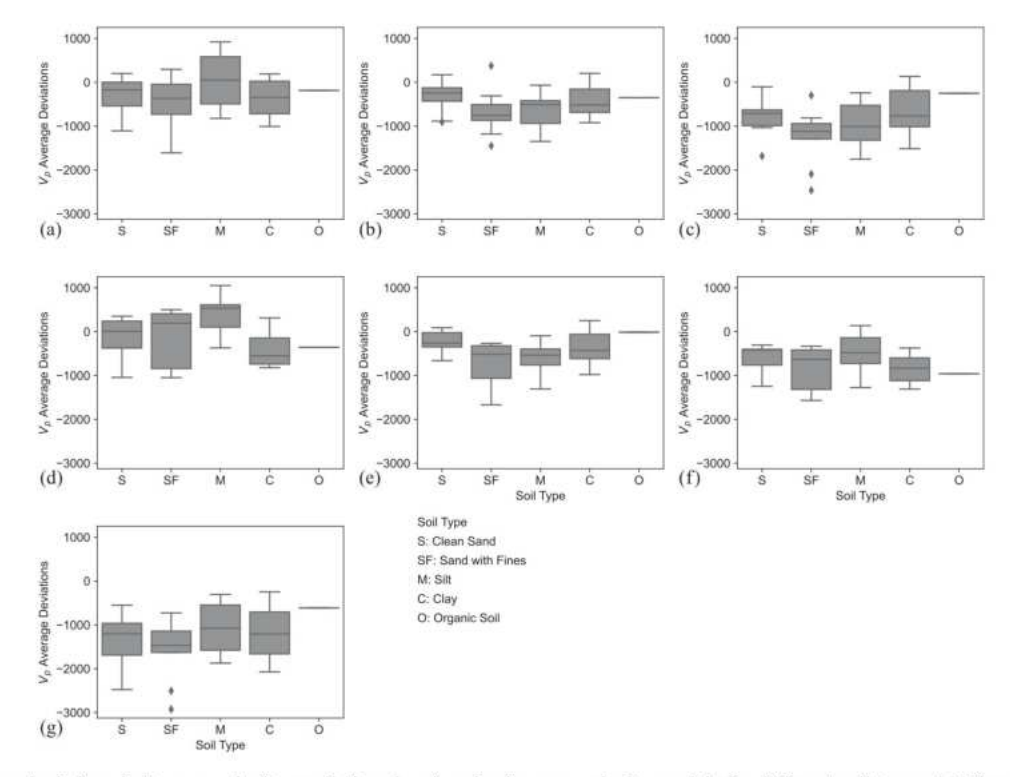


Fig. 14. Average deviations in P wave velocity predictions by six seismic wave velocity models for different soil types: (a) Zimmerman and King (1986); (b) Minshull et al. (1994); (c) weighted equation; (d) three-phase; (e) BGTL; (f) Dou et al. (2017); and (g) time-average models.

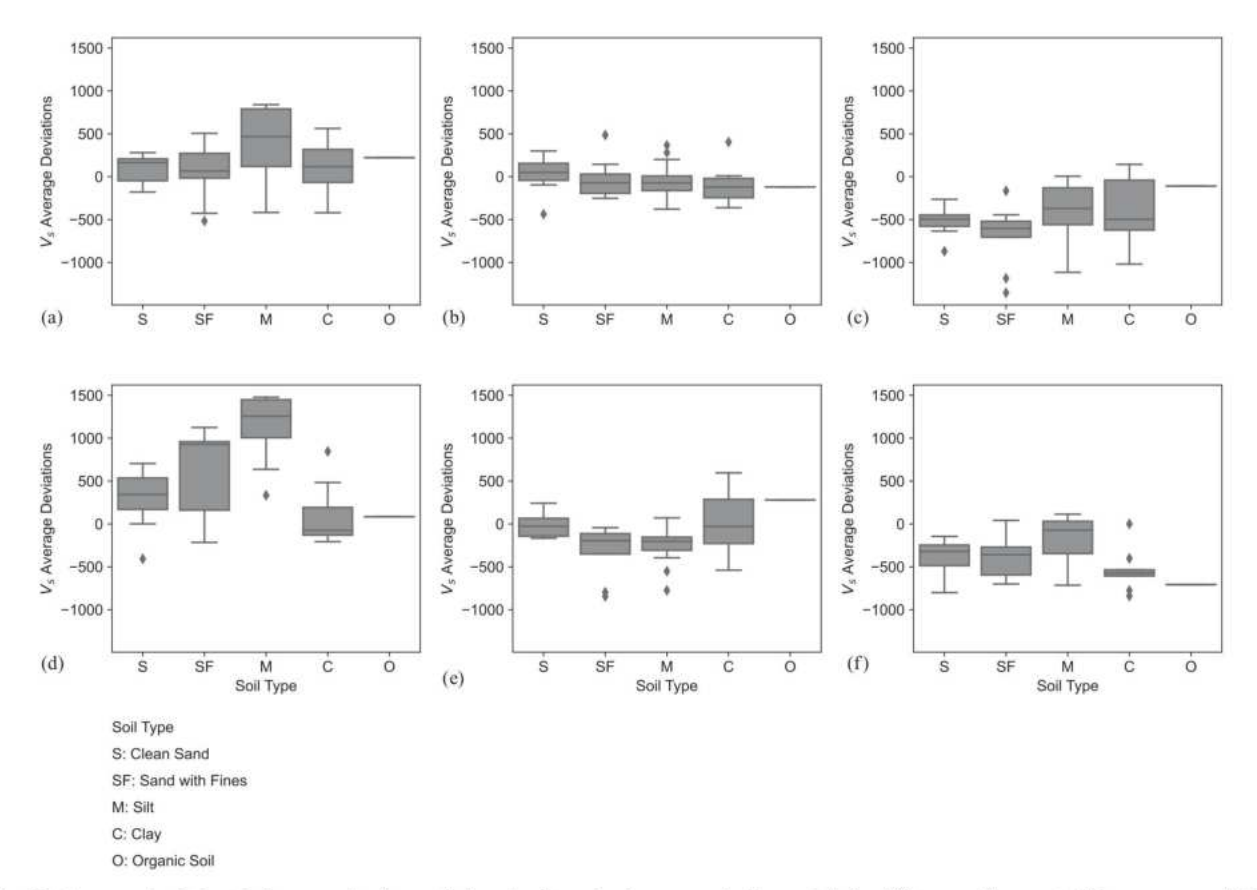


Fig. 15. Average deviations in S wave velocity predictions by five seismic wave velocity models for different soil types: (a) Zimmerman and King (1986); (b) Minshull et al. (1994); (c) weighted equation; (d) three-phase; (e) BGTL; and (f) Dou et al. (2017) models.

14 show the P wave and S wave velocity data. Figs. 10 and 11 show five examples from 41 data sets of the predicted values for the seven models for the P wave velocities and six models for the S wave velocities for different soil types, which include clean sand, sand with fines, silt, clay, and organic soil. The prediction results from different seismic wave velocity models depended on their theory and assumptions. For example, as shown in Fig. 10(b), the Zimmerman and King (1986) model shows a good match with sand with fines samples from Li (2009). This sample has an initial moisture content ($\theta_0 = 27\%$) and porosity ($\phi = 0.5$), which align with the application range $\phi \in [0.3, 0.5]$. Figs. 12–15 show the RMSE and average deviations for the seismic wave velocity models for different soil types for P and S wave velocity predictions, respectively.

Data Availability Statement

Some or all data, models, or codes generated or used during the study are available in a repository or online in accordance with funder data retention policies. Ji, X., Liew, M., and Xiao, M. 2022. Supplementary data for "Statistical Evaluation of Seismic Wave Velocity Models of Permafrost." Penn State Data Commons. http://doi.org/10.26208/6H4X-JC81.

Acknowledgments

This study is supported by the National Science Foundation under Grants CMMI-2034363, CMMI-2034366, and ICER-1927718. Dr. Min Liew provided advice on data collection.

Author contributions: Xiaohang Ji: Conceptualization, methodology, software, formal analysis, investigation, writing the original draft, and visualization. Ming Xiao: Conceptualization, methodology, validation, writing (review and editing), visualization, supervision, project administration, and funding acquisition. Eileen Martin: Conceptualization, writing (review and editing), project administration, and funding acquisition. Tieyuan Zhu: Conceptualization, writing (review and editing), project administration, and funding acquisition.

References

Anderson, D. M., and A. R. Tice. 1972. "Predicting unfrozen water contents in frozen soils from surface area measurements." *Highway Res. Rec.* 393: 12–18.

Berryman, J. G. 1995. "Mixture theories for rock properties." In Rock physics and phase relations: A handbook of physical constants. Vol. 3, edited by T. J. Ahrens, 205–228. Chichester, UK: Wiley.

Biot, M. A. 1956. "Theory of propagation of elastic waves in a fluid-saturated porous solid. II. Higher frequency range." J. Acoust. Soc. Am. 28 (2): 179–191. https://doi.org/10.1121/1.1908241.

Carcione, J. M., and G. Seriani. 1998. "Seismic and ultrasonic velocities in permafrost." *Geophys. Prospect.* 46 (4): 441–454. https://doi.org/10 .1046/j.1365-2478.1998.1000333.x.

Castagna, J. P., M. L. Batzle, and R. L. Eastwood. 1985. "Relationships between compressional-wave and shear-wave velocities in clastic silicate rocks." Geophysics 50 (4): 571–581. https://doi.org/10.1190/1.1441933.

Chen, K., M. Jin, G. Li, Y. Liu, J. Lu, Y. Zhao, and Q. Yu. 2023. "Thermal performance and heat transfer process of an expressway embankment

- with horizontal-thermosyphons in permafrost regions." Cold Reg. Sci. Technol. 212: 103887. https://doi.org/10.1016/j.coldregions.2023
- Christ, M., Y.-C. Kim, and J.-B. Park. 2009. "The influence of temperature and cycles on acoustic and mechanical properties of frozen soils." KSCE J. Civ. Eng. 13 (3): 153–159. https://doi.org/10.1007/s12205 -009-0153-1.
- Dall'Amico, M., S. Endrizzi, S. Gruber, and R. Rigon. 2011. "A robust and energy-conserving model of freezing variably-saturated soil." *Cryosphere* 5 (2): 469–484. https://doi.org/10.5194/tc-5-469-2011.
- Dou, S., S. Nakagawa, D. Dreger, and J. Ajo-Franklin. 2016. "A rock-physics investigation of unconsolidated saline permafrost: P-wave properties from laboratory ultrasonic measurements." *Geophysics* 81 (1): WA233–WA245. https://doi.org/10.1190/geo2015-0176.1.
- Dou, S., S. Nakagawa, D. Dreger, and J. Ajo-Franklin. 2017. "An effective-medium model for P-wave velocities of saturated, unconsolidated saline permafrost." *Geophysics* 82 (3): EN33–EN50. https://doi.org/10.1190/geo2016-0474.1.
- Dvorkin, J., and A. Nur. 1998. "Time-average equation revisited." Geophysics 63 (2): 460–464. https://doi.org/10.1190/1.1444347.
- Eberhart-Phillips, D., D.-H. Han, and M. D. Zoback. 1989. "Empirical relationships among seismic velocity, effective pressure, porosity, and clay content in sandstone." *Geophysics* 54 (1): 82–89. https://doi.org/10.1190/1.1442580.
- Ferrero, A. M., A. Godio, M. Migliazza, L. Sambuelli, A. Segalini, and A. Théodule. 2014. "Geotechnical and geophysical characterization of frozen granular material." In *Landslides in cold regions in the context of climate change*, edited by W. Shan, Y. Guo, F. Wang, H. Marui, and A. Strom, 205–218. Cham, Switzerland: Springer.
- Fu, R., J. Zhang, and Z. Hou. 1983. "Ultrasonic velocities in frozen soil." In Proc. 4th Int. Conf. on Permafrost, 311–315. Washington, DC: The National Academies Press.
- Gassmann, F. 1951. "Elastic waves through a packing of spheres." Geophysics 16 (4): 673–685. https://doi.org/10.1190/1.1437718.
- Ge, X., Z. Yang, and B. Still. 2013. "Mechanical properties of naturally frozen ice-rich silty soils." In *Mechanical properties of frozen soil*, 124–139. West Conshohocken, PA: ASTM International.
- Hashin, Z., and S. Shtrikman. 1963. "A variational approach to the theory of the elastic behaviour of multiphase materials." J. Mech. Phys. Solids 11 (2): 127–140. https://doi.org/10.1016/0022-5096(63) 90060-7.
- Haynes, F. D., and J. A. Karalius. 1977. Effect of temperature on the strength of frozen silt (No. 77). Hanover, NH: Dept. of Defense, Dept. of the Army, Corps of Engineers, Cold Regions Research and Engineering Laboratory.
- Hill, R. 1952. "The elastic behaviour of a crystalline aggregate." Proc. Phys. Soc. London, Sect. A 65 (5): 349. https://doi.org/10.1088/0370 -1298/65/5/307.
- Hivon, E., and D. C. Sego. 1990. "Determination of the unfrozen water content of saline permafrost using time-domain reflectometry (TDR)." In Proc. 5th Canadian Permafrost Conf., 257–262. Quebec, Canada: University of Laval.
- Hoyer, W. A., S. O. Simmons, M. M. Spann, and A. T. Watson. 1975. "Evaluation of permafrost with logs." In *Proc.*, SPWLA 16th Annual Logging Symp. Richardson, TX: One Petro.
- Hu, G., L. Zhao, X. Zhu, X. Wu, T. Wu, R. Li, C. Xie, and J. Hao. 2020. "Review of algorithms and parameterizations to determine unfrozen water content in frozen soil." *Geoderma* 368: 114277. http://doi.org/10.1016/j.geoderma.2020.114277.
- Kim, Y., D. Chae, K. Kim, and W. Cho. 2016. "Physical and mechanical characteristics of frozen ground at various sub-zero temperatures." KSCE J. Civ. Eng. 20 (6): 2365–2374. https://doi.org/10.1007/s12205 -015-0542-6.
- King, M. S., R. W. Zimmerman, and R. F. Corwin. 1988. "Seismic and electrical properties of unconsolidated Permafrost." Geophys. Prospect. 36 (4): 349–364. https://doi.org/10.1111/j.1365-2478.1988 .tb02168.x.
- Kozlowski, T. 2007. "A semi-empirical model for phase composition of water in clay-water systems." *Cold Reg. Sci. Technol.* 49: 226–236. https://doi.org/10.1016/j.coldregions.2007.03.013.

- Kurfurst, P. J. 1976. "Ultrasonic wave measurements on frozen soils at permafrost temperatures." Can. J. Earth Sci. 13 (11): 1571–1576. https:// doi.org/10.1139/e76-163.
- Kuster, G. T., and M. N. Toksöz. 1974. "Velocity and attenuation of seismic waves in two-phase media: Part I. Theoretical formulations." Geophysics 39 (5): 587–606. https://doi.org/10.1190/1.1440450.
- Lai, Z., X. Zhao, R. Tang, and J. Yang. 2021. "Electrical conductivity-based estimation of unfrozen water content in saturated saline frozen sand." Adv. Civ. Eng. 2021: 8881304. https://doi.org/10.1155/2021/8881304.
- Leclaire, P., F. Cohen-Ténoudji, and J. Aguirre-Puente. 1994. "Extension of Biot's theory of wave propagation to frozen porous media." J. Acoust. Soc. Am. 96 (6): 3753–3768. https://doi.org/10.1121/1 411336
- Lee, M. W. 2002. "Biot-Gassmann theory for velocities of gas hydratebearing sediments." Geophysics 67 (6): 1711–1719. https://doi.org/10 1190/11527072.
- Lee, M. W., D. R. Hutchinson, T. S. Collett, and W. P. Dillon. 1996. "Seismic velocities for hydrate-bearing sediments using weighted equation." J. Geophys. Res.: Solid Earth 101 (B9): 20347–20358. https://doi.org/10.1029/96JB01886.
- Li, H. 2009. "Experimental and numerical study of sonic wave propagation in freezing sand and silt." Ph.D. thesis, Dept. of Mining and Geological Engineering, Univ. of Alaska Fairbanks.
- Li, X., and X. Li. 2023. "A soil freezing-thawing model based on thermodynamics." Cold Reg. Sci. Technol. 211: 103867. https://doi.org/10 .1016/j.coldregions.2023.103867.
- Li, X., X. Li, and J. Liu. 2023a, In press. "A dynamic soil freezing characteristic curve model for frozen soil." J. Rock Mech. Geotech. Eng. http://doi.org/10.1016/j.jrmge.2023.09.008.
- Li, X., S.-F. Zheng, M. Wang, and A.-Q. Liu. 2023b. "The prediction of the soil freezing characteristic curve using the soil water characteristic curve." Cold Reg. Sci. Technol. 212: 103880. https://doi.org/10.1016/j .coldregions.2023.103880.
- Li, Z., J. Chen, and M. Sugimoto. 2020. "Pulsed NMR measurements of unfrozen water content in partially frozen soil." J. Cold Reg. Eng. 34 (3): 04020013. https://doi.org/10.1061/(ASCE)CR.1943-5495 .0000220.
- Liew, M., X. Ji, M. Xiao, L. Farquharson, D. Nicolsky, V. Romanovsky, M. Bray, X. Zhang, and C. McComb. 2022. "Synthesis of physical processes of permafrost degradation and geophysical and geomechanical properties of permafrost." *Cold Reg. Sci. Technol.* 198: 103522. https:// doi.org/10.1016/j.coldregions.2022.103522.
- Lu, J., W. Pei, X. Zhang, J. Bi, and T. Zhao. 2019. "Evaluation of calculation models for the unfrozen water content of freezing soils." *J. Hydrol.* 575: 976–985. https://doi.org/10.1016/j.jhydrol.2019.05.031.
- Lyu, C., S. A. G. Amiri, G. Grimstad, K. V. Høyland, and T. Ingeman-Nielsen. 2020. "Comparison of geoacoustic models for unfrozen water content estimation." *J. Geophys. Res.: Solid Earth* 125 (10): e2020JB019766, https://doi.org/10.1029/2020JB019766.
- McGaw, R. W., R. L. Berg, and J. W. Ingersoll. 1983. "An investigation of transient processes in an advancing zone of freezing." In Proc., 4th Int. Conf. on Permafrost, 821–825. Washington, DC: The National Academies Press.
- McKenzie, J. M., C. I. Voss, and D. I. Siegel. 2007. "Groundwater flow with energy transport and water-ice phase change: Numerical simulations, benchmarks, and application to freezing in peat bogs." Adv. Water Resour. 30 (4): 966–983. https://doi.org/10.1016/j.advwatres .2006.08.008.
- Meng, Q., D. Li, J. Chen, A. Xu, and S. Huang. 2008. "Experimental research on physical-mechanical characteristics of frozen soil based on ultrasonic technique." In Vol. 2 of *Proc.*, 9th Int. Conf. on Permafrost, 1179–1183. Fairbanks, Alaska: University of Alaska.
- Michalowski, R. L. 1993. "A constitutive model of saturated soils for frost heave simulations." Cold Reg. Sci. Technol. 22: 47–63. https://doi.org/10.1016/0165-232X(93)90045-A.
- Mindlin, R. D. 1949. "Compliance of elastic bodies in contact." J. Appl. Mech. 16: 259–268. https://doi.org/10.1115/1.4009973.
- Minshull, T. A., S. C. Singh, and G. K. Westbrook. 1994. "Seismic velocity structure at a gas hydrate reflector, offshore western Colombia, from full

- waveform inversion." J. Geophys. Res.: Solid Earth 99 (B3): 4715–4734. https://doi.org/10.1029/93JB03282.
- Nakano, Y., and R. Arnold. 1973. "Acoustic properties of frozen Ottawa sand." Water Resour. Res. 9 (1): 178–184. https://doi.org/10.1029 /WR009i001p00178.
- Nakano, Y., and N. H. Froula. 1973. "Sound and shock transmission in frozen soils." In *Proc.*, 2nd Int. Conf. on Permafrost, 359–369. Washington, DC: National Academy of Sciences.
- Nakano, Y., R. J. Martin III, and M. Smith. 1972. "Ultrasonic velocities of the dilatational and shear waves in frozen soils." Water Resour. Res. 8 (4): 1024–1030. https://doi.org/10.1029/WR008i004p01024.
- Nobes, D. C., H. Villinger, E. E. Davis, and L. K. Law. 1986. "Estimation of marine sediment bulk physical properties at depth from seafloor geophysical measurements." J. Geophys. Res.: Solid Earth 91 (B14): 14033–14043. https://doi.org/10.1029/JB091iB14p14033.
- Oliphant, J. L., A. R. Tice, and Y. Nakano. 1983. "Water migration due to a temperature gradient in frozen soil." In *Proc.*, 4th Int. Conf. on Permafrost, 951–956. Washington, DC: The National Academies Press.
- Pearson, C. F., P. M. Halleck, P. L. McGuire, R. Hermes, and M. Mathews. 1983. "Natural gas hydrate deposits: A review of in situ properties." J. Phys. Chem. 87 (21): 4180–4185. https://doi.org/10.1021/j100244 a041
- Qiu, E., X. Wan, M. Qu, L. Zheng, C. Zhong, F. Gong, and L. Liu. 2020. "Estimating unfrozen water content in frozen soils based on soil particle distribution." J. Cold Reg. Eng. 34 (2): 04020002. https://doi.org/10 .1061/(ASCE)CR.1943-5495.0000208.
- Radd, F. J., and L. H. Wolfe. 1979. "Ice lens structures, compression strengths and creep behavior of some synthetic frozen silty soils." Dev. Geotech. Eng. 26: 169–183. https://doi.org/10.1016/B978-0-444 -41782-4.50020-8.
- Ren, J., S. K. Vanapalli, and Z. Han. 2017. "Soil freezing process and different expressions for the soil-freezing characteristic curve." Sci. Cold Arid Reg. 9 (3): 221–228.
- Reuss, A. 1929. "Berechnung der Fliessgrenze von Mischkristallen auf Grund der Plastizitätsbedingung für Einkristalle." J. App. Mathemat. Mech. 9: 49–58. http://dx.doi.org/10.1002/zamm.19290090104.
- Schön, J. 2011. Vol. 8 of Physical properties of rocks: A workbook. Oxford. UK: Elsevier.
- Smith, M. W., and A. R. Tice. 1988. "Measurement of the unfrozen water content of soils." In Comparison of NMR (nuclear magnetic resonance) and TDR (time domain reflectometry) methods. Hanover, NH: Cold Regions Research and Engineering Lab.
- Timur, A. 1968. "Velocity of compressional waves in porous media at permafrost temperatures." Geophysics 33: 584–595. https://doi.org/10 .1190/1.1439954.
- Thimus, J. F., J. Aguirre-Puente, and F. Cohen-Tenoudji. 1991. "Determination of unfrozen water content of an overconsolidated clay down to -160°C by sonic approaches-comparison with classical methods." Ground Freezing 91: 83–88.

- van Genuchten, M. T. 1980. "A closed-form equation for predicting the hydraulic conductivity of unsaturated soils." Soil Sci. Soc. Am. J. 44 (5): 892–898. https://doi.org/10.2136/sssaj1980.03615995004400050002x.
- Voigt, W. 1928. Lerrbuch der Kristallphysik. Leipzig, Germany: Teubner. Wang, D.-Y., Y.-L. Zhu, W. Ma, and Y.-H. Niu. 2006. "Application of ultrasonic technology for physical-mechanical properties of frozen soils." Cold Reg. Sci. Technol. 44 (1): 12–19. https://doi.org/10.1016/j.coldregions.2005.06.003.
- Watanabe, K., and Y. Osada. 2017. "Simultaneous measurement of unfrozen water content and hydraulic conductivity of partially frozen soil near 0°C." Cold Reg. Sci. Technol. 142: 79–84. https://doi.org/10.1016/j.coldregions.2017.08.002.
- Watanabe, K., and T. Wake. 2009. "Measurement of unfrozen water content and relative permittivity of frozen unsaturated soil using NMR and TDR." Cold Reg. Sci. Technol. 59 (1): 34–41. https://doi.org/10.1016/j.coldregions.2009.05.011.
- Wen, Z., W. Ma, W. Feng, Y. Deng, D. Wang, Z. Fan, and C. Zhou. 2012. "Experimental study on unfrozen water content and soil matric potential of Qinghai-Tibetan silty clay." *Environ. Earth Sci.* 66 (5): 1467–1476. https://doi.org/10.1007/s12665-011-1386-0.
- Wood, A. B. 1941. A textbook of sound. London: G. Bell and Sons.
- Wyllie, M. R. J., A. R. Gregory, and G. H. F. Gardner. 1958. "An experimental investigation of factors affecting elastic wave velocities in porous media." *Geophysics* 23 (3): 459–493. https://doi.org/10.1190/1.1438493.
- Yang, Z. J., B. Still, and X. Ge. 2015. "Mechanical properties of seasonally frozen and permafrost soils at high strain rate." *Cold Reg. Sci. Technol.* 113: 12–19. https://doi.org/10.1016/j.coldregions.2015.02.008.
- Zhang, F., Z. J. Yang, B. Still, J. Wang, H. Yu, H. Zubeck, T. Petersen, and L. Aleshire. 2018. "Elastic properties of saline permafrost during thawing by bender elements and bending disks." Cold Reg. Sci. Technol. 146: 60–71. https://doi.org/10.1016/j.coldregions.2017.11.014.
- Zhang, M., W. Pei, S. Li, J. Lu, and L. Jin. 2017. "Experimental and numerical analyses of the thermo-mechanical stability of an embankment with shady and sunny slopes in a permafrost region." Appl. Therm. Eng. 127: 1478–1487. https://doi.org/10.1016/j.applthermal eng.2017.08.074.
- Zhang, M., X. Zhang, Y. Lai, J. Lu, and C. Wang. 2020. "Variations of the temperatures and volumetric unfrozen water contents of fine-grained soils during a freezing-thawing process." *Acta Geotech*. 15: 595–601. https://doi.org/10.1007/s11440-018-0720-z.
- Zhang, M., X. Zhang, J. Lu, W. Pei, and C. Wang. 2019. "Analysis of volumetric unfrozen water contents in freezing soils." Exp. Heat Transfer 32 (5): 426–438. https://doi.org/10.1080/08916152.2018.1535528.
- Zhu, Y., and D. L. Carbee. 1984. "Uniaxial compressive strength of frozen silt under constant deformation rates." Cold Reg. Sci. Technol. 9 (1): 3– 15. https://doi.org/10.1016/0165-232X(84)90043-0.
- Zimmerman, R. W., and M. S. King. 1986. "The effect of the extent of freezing on seismic velocities in unconsolidated permafrost." Geophysics 51: 1285–1290. https://doi.org/10.1190/1.1442181.